MATHEMATICAL MODELLING OF THE HIGH TEMPERATURE CONSTITUTIVE BEHAVIOUR OF AS-CAST AA5182 ALUMINUM ALLOY

by

ABDUL-RAHMAN ALHASSAN-ABU

M.Sc., University of Matanzas "Camilo Cienfuegos", Matanzas, Cuba

A THESIS SUBMITTED IN PARTIAL FULFILLMENT OF

THE REQUIREMENTS FOR THE DEGREE OF

MASTER OF APPLIED SCIENCE

in

THE FACULTY OF GRADUATE STUDIES

(DEPARTMENT OF METALS AND MATERIALS ENGINEERING)

We accept this thesis as conforming

to the required standard

THE UNIVERSITY OF BRITISH COLUMBIA

February, 2001

In presenting this thesis in partial fulfilment of the requirements for an advanced degree at the University of British Columbia, I agree that the Library shall make it freely available for reference and study. I further agree that permission for extensive copying of this thesis for scholarly purposes may be granted by the head of my department or by his or her representatives. It is understood that copying or publication of this thesis for financial gain shall not be allowed without my written permission.

Department of METALS & MATERIALS ENGINEERING

The University of British Columbia
Vancouver, Canada

Date March 6, 2001.

ABSTRACT

Compression, tension and cyclical compression-tension tests were done using the Gleeble 1500 thermomechanical simulator at the University of British Columbia to measure the constitutive behaviour in an as-cast AA5182 aluminum alloy. The temperatures (i.e., 250-500°C) and strain rates (1E-5 - 1s^{-1}) used for the tests were chosen to represent typical conditions experienced in the solid phase during DC casting due to thermally induced deformations which occur during cooling. Using the measurement results, a constitutive relationship using Garofalo's hyperbolic sine relationship was developed and tabular data relating stress to strain at various strain rates and temperatures was also generated. The experiments done on the Gleeble 1500 machine were also simulated using the commercial finite element code ABAQUS^{TM}. Various methods within ABAQUS were used to numerically simulate the inelastic behaviour of the material during the deformation and included a hyperbolic sine creep law, strain rate dependent plasticity using tabular data and strain rate independent plasticity. The results predicted by the models developed within ABAQUS were then verified by comparing the predicted results to measurements made using the Gleeble 1500 thermal mechanical simulator under different temperature and strain rate conditions than originally used to develop the constitutive relationships. The results indicated that within ABAQUS the most accurate way to simulate stress strain behaviour that occurs during DC casting is to use strain rate dependent plasticity.

TABLE OF CONTENTS

LIST OF TABLES

LIST OF FIGURES

NOMENCLATURE

α Fitting parameter in the hyperbolic-sine equation

β Fitting parameter in the exponential equation

ε strain

ε_c diametric strain

ε_L lengthwise strain

ε_{creep} creep strain

ε_{el} elastic strain

ε_{pl} plastic strain

ε_{total} total strain

$\varepsilon_{thermal}$ thermal strain

$\overline{\varepsilon}_{pl}$ equivalent plastic strain

$\dot{\overline{\varepsilon}}^{pl}$ equivalent plastic strain rate

$\overline{\varepsilon}_{cr}$ equivalent creep strain

$\dot{\overline{\varepsilon}}_{cr}$ uniaxial equivalent creep strain rate

$\dot{\varepsilon}_{mean}$ mean strain rate

$\dot{\varepsilon}$ strain rate

$\dot{\varepsilon}_{el}$ elastic strain rate

$\dot{\varepsilon}_{pl}$ plastic strain rate

σ flow stress

σ_A stress (auxiliary load cell)

σ_F stress (standard load cell)

σ^0 static yield strength

σ_0 initial yield stress

σ_s steady state stress

A instantaneous cross-sectional area

A, A', A'' constants

ΔH activation energy

D_{el} constitutive matrix

D_{RT} diameter at room temperature

$\delta D_{thermal}$ change in diameter due to thermal expansion

D_0 diameter at start of deformation

E Young's Modulus

F Load

k dimensionless material constant

K material constant

L_o initial length

L_{RT} length at room temperature

m material constant

m strain rate sensitivity

n temperature dependent parameter

$\delta L_{thermal}$ change in length due to thermal expansion

Q_{def} activation energy

$\tilde{q}$ Von Mises equivalent stress

r   radius

R   universal gas constant

T temperature in Kelvin

T_{def} deformation temperature

T_m melting point

t   time

t total time

θ temperature in Kelvin

θ^z value of absolute zero

U   displacement in the x-direction

V   displacement in the y-direction

V_o volume prior to deformation

V volume after deformation

W_i and W_j weighting coefficients

Z Zener-Hollomon parameter

ACKNOWLEDGEMENT

Chapter I - Introduction

1.1 DC casting process

The Canadian aluminum industry is presently the third largest supplier of aluminum, producing approximately 2.3 million tonnes of primary aluminum per year (11% of the world capacity). The primary technology used to cast sheet products made from aluminum is the semi-continuous Direct Chill (DC) casting process which produces an ingot which is subsequently rolled into sheet products. Although this casting process has been used almost exclusively to produce aluminum sheet ingot during the past 60 years, relatively little fundamental work has been done to optimize the design of the casting process from the standpoint of final ingot quality. As a result, there has been a trend to try and quantify the influence of casting parameters on the quality of the ingots being produced through the use of mathematical models. In particular, the start-up phase of the process is particularly complicated, as the ingot surface temperature, water flow rate in the secondary cooling regime, and casting speed are all changing with time.

As shown in Figure 1.1, the DC casting process, for producing sheet ingots, consists of an open rectangular mould which confines the molten metal and distributes the cooling water around the ingot via the water chamber.
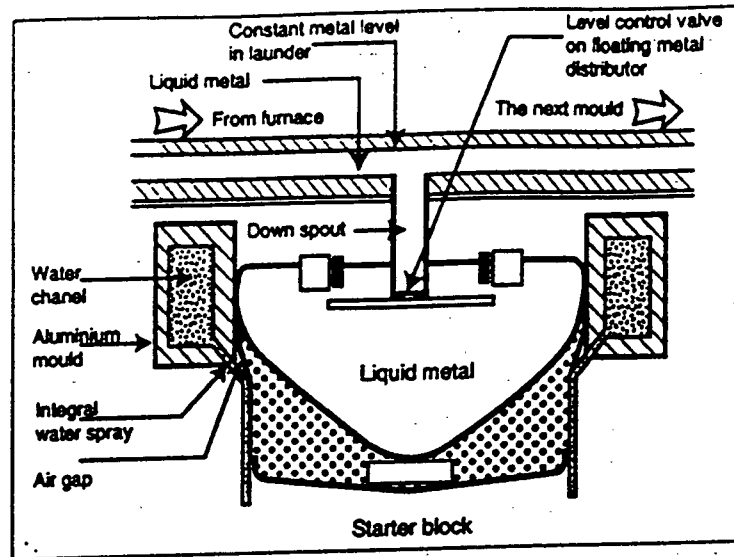
Figure 1.1 – Schematic of the DC casting process [1].

On start-up, a bottom block mounted on a horizontal lowering table closes off the mould [1,2,3]. Once the metal has reached a certain level in the mould, the bottom block is lowered. A superheated liquid metal is poured via a nozzle through a distribution bag into the liquid pool at the top of the mould and the metal level in the mould is kept constant through the use of a non-contact metal level sensor. The aluminum is subjected to both primary cooling in the mould as well as secondary cooling in the water chill area below the mould. The primary mould cooling accounts for about 10-20 % of the heat extracted from the aluminum ingot whereas the secondary water cooling accounts for about 80-90% of the heat extracted from the ingot at steady state as shown in Figure 1.2. In addition, a significant amount of heat is extracted from the bottom block through the base of the ingot during the transient start-up phase.

2
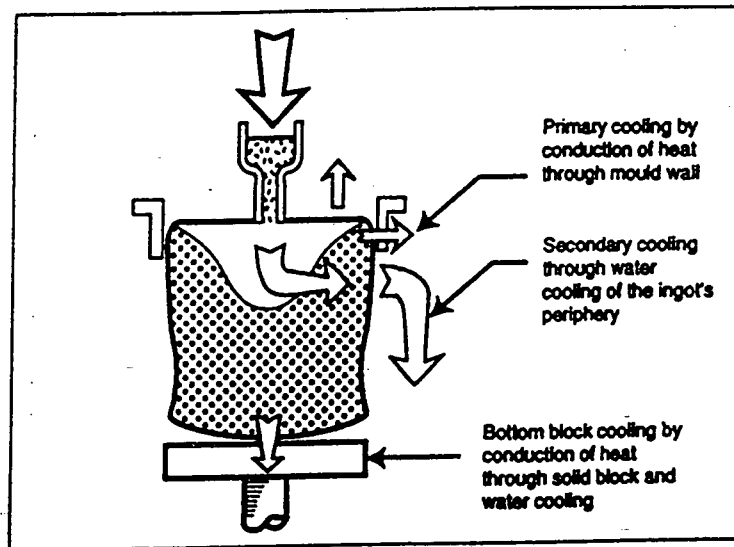
Figure 1.2 - Schematic illustration of primary and secondary cooling during conventional DC ingot casting [4].

The most critical phase of the DC casting process is start-up, where the casting velocity and water flow rate are gradually adjusted and the liquidus and solidus profile within the ingot evolve with time. During this start-up phase, a phenomenon known as butt curl occurs which is a macroscopic deformation of the ingot, characterized by a bowing up of the shell against the bottom block. The most pronounced effect occurs near the narrow faces of the ingot as shown in Figure 1.3. The resultant gap induced by this deformation may reach a magnitude of ~45mm [4].
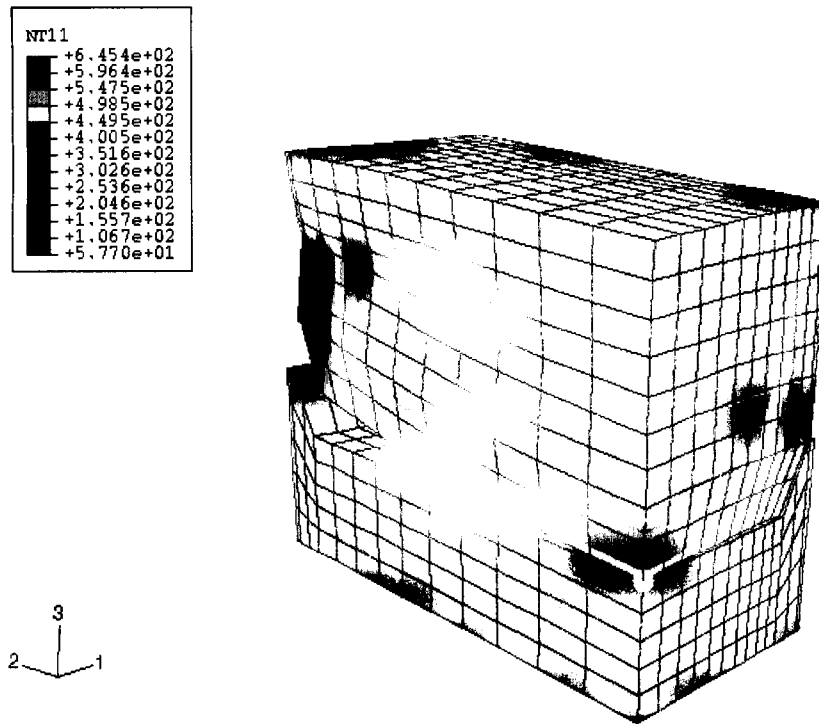
Figure 1.3 - Predicted thermal distribution and ingot butt curl after 500s using a coupled thermal-stress model during DC casting (displacement magnification of 2.078) [4].

During the initial stage of the casting process, once the process of solidification has commenced, the bottom block is lowered into the casting pit and out of the bottom of the mould at a constant casting speed (usually ~1 mm/s). For a given alloy, the position and shape of the liquidus and solidus isotherms with respect to the mould are dependent on parameters such as the superheat in the liquid metal, the method of introducing the metal into the liquid sump, the cooling spray configuration, and the casting speed [2].

The DC casting process is semi-continuous thus, once the slab or billet reaches the desired length, which generally corresponds to the capacity of the furnace and to the depth of the casting pit, the casting process is stopped.

One of the technical challenges in using the DC casting technology, is the ability to cast high strength sheet alloys (i.e., AA5xxx and AA6xxx) economically and free from defects. These high strength alloys are particularly difficult to cast as they are very prone to hot tearing or cracking, especially during the start-up phase, thereby resulting in a substantial yield loss and low recovery rates.

1.2 Thermo-mechanical modeling of the DC casting process

In an effort to understand what is occurring during ingot solidification and optimize process parameters during DC casting so as to improve both productivity and recovery rates, off-line thermal-stress models have been developed over the past decade.

Although significant progress has been made over the past few years in the simulation of this casting process, there is still some difficulty in predicting with certainty which conditions will cause a hot tear to occur and which will not. Much of this is due to the lack of a good hot tearing model as well as the lack of information about as-cast material behaviour in both the mushy zone as well as high temperature regimes during solidification. As a result it is critical to measure the as-cast material response under similar temperature and strain rate regimes as encountered during DC casting and develop quantitative relationships that will describe the constitutive behaviour of the material being cast from its coherency point, where it first begins to behave like a solid, down to room temperature.

This project is part of another larger project at The University of British Columbia whose goal is to develop a 3-D thermal-stress model of the start-up phase for the DC

casting process using the commercial FEM software package ABAQUS™[†]. Therefore, another objective of this project is to investigate the numerical methods available within ABAQUS to model the material constitutive behaviour in the solid state as it cools to room temperature.

[1†] ABAQUS is a registered trademark of Hibbitt, Karlsson & Sorensen Inc.

Chapter II - Literature Review

2.1 DC casting of aluminum alloys

2.1.1 Microstructural development of AA5182 during solidification

Aluminum alloy AA5182 is a medium strength non-heat treatable alloy, which is used in a variety of applications including beverage can ends and inner body panels for automotive applications. The main alloy addition in AA5182 is Mg, which provides solid solution strengthening. During DC casting, solidification of AA5182 begins with the formation of the primary α-Al dendrites. Under equilibrium cooling conditions, these dendrites start to form at 637°C. The dendrites become coherent (i.e., the continuous dendritic network offers a resistance to mechanical deformation) at a temperature of $\sim$ 632°C. As the material continues to cool the first eutectic reaction occurs at 623°C where the liquid forms primary α-Al and Al_6(Fe, Mn) when the material is ~40% solid. Precipitation of Mg_2Si starts at 582°C when the material is 93% solid and precipitation of complex eutectic phases occurs when the material is 98% solid at 560°C according to the following reaction [5]:

$$\text{Liquid} \rightarrow \quad Al + Mg_2Si + Al_3Fe + Al_8Mg_5 \qquad (2.1)$$
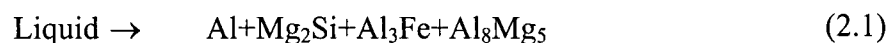
Solidification ends at ~536°C.

Figure 2.1 summarizes the reactions that occur during the solidification process of AA5182.

Ppt. of complex eutectic (560°C)
Liq→Al+Mg$_2$Si+Al$_3$Fe+Al$_8$Mg$_5$

Ppt. of Mg$_2$Si (582°C)
Liq→Al+Mg$_2$Si

End of solidification
(536°C)

Fraction solid (%)

100
90
80
70
60
50
40
30
20
10
0

Eutectic reaction (623°C)
Liq→α-Al+Al$_6$(Fe,Mn)

Dendrite coherency
point (632°C)

Formation of α-Al
(637°C)

725   675   625   575   525   475

Temperature (°C)
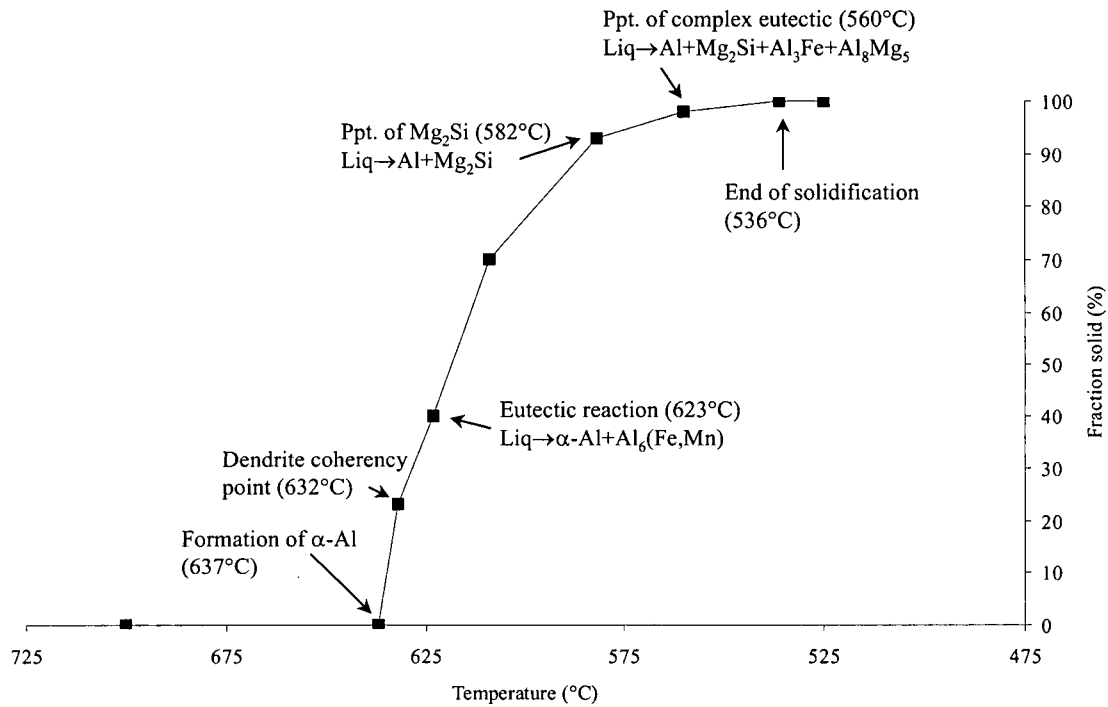
Figure 2.1- Microstructure changes occurring during solidification of AA5182 [5].

In the solid as-cast state, the microstructure of AA5812 consists of primary α-aluminum and eutectic phases (Al$_6$(Fe,Mn), Al$_3$Fe, Al$_8$Mg$_5$) and Mg$_2$Si.

2.1.2 Mechanical properties

During the DC casting process the thermomechanical history experienced throughout the ingot is quite different. At the surface of the sheet ingot the cooling rates are relatively fast (i.e., >1°C/s) whereas in the center of the ingot the cooling rates are relatively slow (i.e. <0.06°C/s) [6]. Hence the rate of deformation experienced is a complex phenomenon and this translates to different strain rates at the surface of the ingot as it cools to room temperature in the order of 1 s^{-1} whereas in the center it is approximately 1.0E-5 s^{-1}.

2.1.2.1 Mushy zone

Attempts to measure the strength of aluminum alloys in their semi-solid or mushy state have been made by Drezet et al. [7] Chu [8] and Ackerman [9]. Drezet et al. measured the behaviour of as-cast alloys AA1201 and AA3104 in the semi-solid state using a rheological test which involved indenting a solidifying alloy with a needle at a constant temperature and strain rate. This technique was originally used by Branswyck et al. [10] to study the semi-solid behaviour of a Zn-Sn 8 wt.% alloy. The measured resistance can then be modeled using a viscoplastic law in a finite element code where the semi-solid material behaviour can be described using the Norton-Hoff law, as shown in equation 2.2.

$$\dot{\varepsilon} = K\left(\frac{\sigma}{\sigma_0}\right)^n \tag{2.2}$$

where $\dot{\varepsilon}$ is the strain rate, σ_0 is the initial yield strength and K, and n are temperature dependent parameters

To assess strain rate sensitivity of semi-solid material, Drezet et al. measured the load increase as a function of the rate of indentation. As shown in Figure 2.2, Drezet et al. found there was a strong strain rate sensitivity in the semi-solid material.

Ackerman et al. used a different technique and recorded the force necessary to separate two cylinders, at a given rate, after they acquired a concentric layer of solidified metal over their entire surface. Using this test, Ackerman et al. found that at temperatures of 650°C, the Al-0.5%Mg aluminum alloy exhibited strong strain rate sensitivity (i.e., m = 0.34) [9].
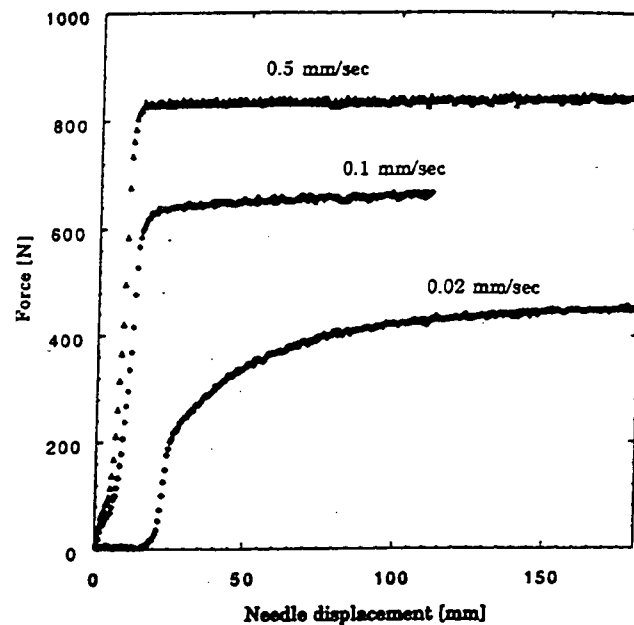
Figure 2.2 - Strain rate sensitivity of AA1201 in the semi-solid regime at 635°C [7].

Although the mechanical behaviour of semi-solid alloys is of great importance for the modelling of thermomechanical stresses and hot tearing during casting, it is usually poorly known.

2.1.2.2 Solid state

In general and for most polycrystalline metals such as in the case of aluminum alloys, the strength of material decreases with increasing temperature. This is due in part to the increased mobility of dislocations at increased temperatures. An important characteristic of high temperature strength (i.e., Temp>$0.5T_m$) is that is must be considered with respect to a time scale as high temperature material behaviour is very sensitive to both strain rate as well as time of exposure. A metal subjected to a constant tensile load at an elevated temperature will undergo a time-dependent progressive deformation, which is called creep [11]. The time dependence of creep deformation usually shows three distinct stages: a primary creep phase during which the creep rate

rapidly decreases. A secondary phase with a constant creep rate and a tertiary phase with increasing creep rate. Primary creep is predominantly transient in which the creep resistance of the material increases by virtue of its own deformation. The secondary phase of creep has an almost constant rate of deformation over time as the processes of strain hardening and recovery balance each other. The third and final stage of creep involves an increasing creep rate just before rupture [11].

The amount of strain which occurs during secondary or steady state creep is generally given by the Garofalo law [12] shown in Equation 2.3:

$$\dot{\varepsilon} = A[\sinh(\alpha\sigma_s)]^n \exp\left(-\frac{Q_{def}}{RT}\right) \tag{2.3}$$

This equation reduces to an exponential relationship at high stresses (i.e. when $\alpha\sigma > 1.2$) as given in Equation 2.4:

$$\dot{\varepsilon} = A' \exp(\beta\sigma_s) \exp\left(-\frac{Q_{def}}{RT}\right) \tag{2.4}$$

Under low stress conditions (i.e., when $\alpha\sigma < 0.8$) the Garofalo law breaks down into a power law dependence of stress as given in Equation 2.5:

$$\dot{\varepsilon} = A'' \sigma_s^n \exp\left(-\frac{Q_{def}}{RT}\right) \tag{2.5}$$

where A, A', A'', n, α and β are material constants that depend on composition, Q_{def} is the activation energy for deformation and R and T are universal gas constant and temperature respectively.

Most of the high temperature material properties reported in the literature for aluminum alloys are for wrought materials [13,14,15] whose microstructure is quite different to that of as-cast materials. The only study in the literature which compared

wrought aluminum alloy high temperature behaviour to as-cast material behaviour was Lu et al. [16]. In their study they used a continuous cooling tensile test method to examine the differences between as-cast and wrought AA7050. The cooling rates chosen in the test represented those typically found during DC casting, and tests were performed at a variety of temperatures ranging from room temperature to 427°C. The test results showed that the measured strength of the as-cast AA7050 material was significantly lower than that of wrought material at low temperature, with the difference becoming smaller at high temperatures, as shown in Figure 2.3.
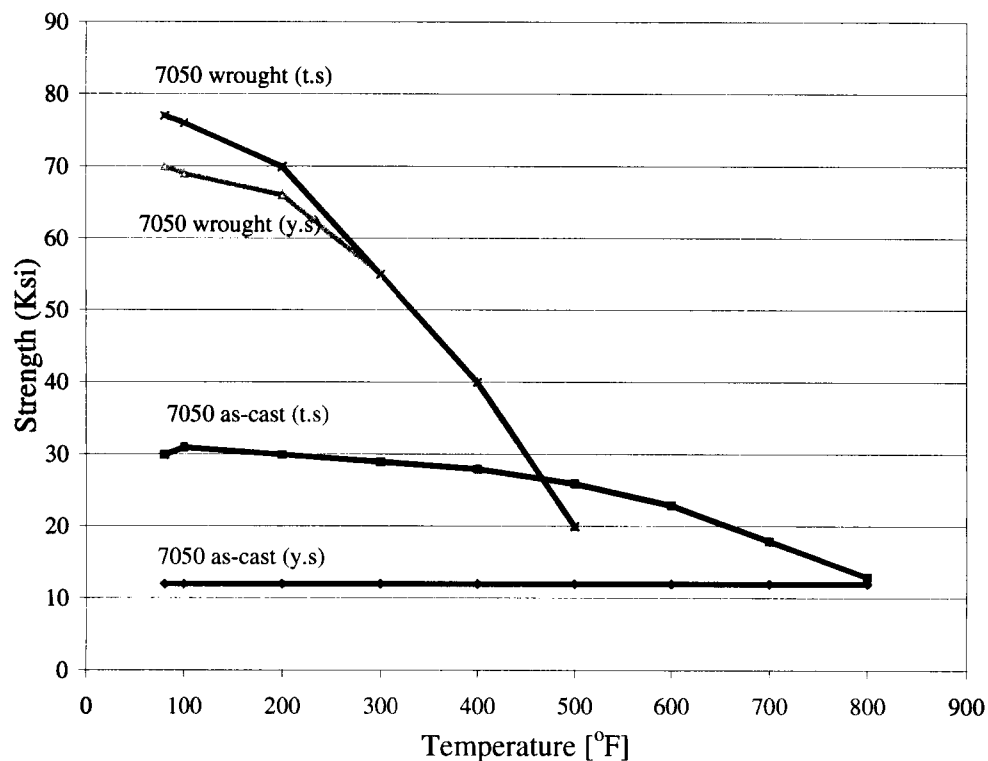
Figure 2.3 - Strength difference between as-cast and wrought AA7050 alloy [16].

A difference in mechanical properties may be expected between as-cast and wrought aluminum alloys due to the difference in the grain size and size and distribution of the precipitates in the matrix, with the grain size and precipitates in the as-cast material

12

being significantly larger. However, it is not clear from this study if the measured difference in the high temperature behaviour, especially at low temperatures, was due to the presence of very fine precipitates in the wrought material which subsequently dissolved at higher temperatures. This study confirms that the thermomechanical behaviour of as-cast materials can be different to that of wrought materials and constitutive relationships used to model the DC casting process should be developed using as-cast material.

Although the constitutive behaviour of as-cast AA5182 was not found in the literature, a few studies have been done to measure and model the constitutive behaviour of wrought AA5182 [17, 18, 19]. These constitutive models were generally developed for hot deformation operations and the strain rates are typically much higher than experienced in DC casting. Chen et al. [19] were the only researchers who made some measurements using wrought AA5182 where the strain rates and temperatures were representative of those found in DC casting.

2.2 Thermomechanical models of the DC casting process

The first generation of mathematical models developed to simulate the DC casting process were fairly simplified and included only the thermal changes that occurred in the ingot as it solidified. In these models, initial attempts were made to quantify the heat transfer to the mould as well as the water spray and bottom block.

One of the first was developed by Peel and Pengelly [20] which was developed based on temperature measurements in the mould and was later modified to incorporate experimental measurements made in the mould and the secondary water cooling regime.

Weckman and Niessen's [21] model of heat flow during DC casting of aluminum was the first to include quantification of the water spray heat transfer coefficients. By measuring the temperature distribution from two separate casts of AA6063, they were able to calculate the heat flux of the secondary water cooling system during DC casting. Included in their expression was the influence of water flow rate on the heat transfer coefficient.

Watanabe and Hayashi [22] were some of the first researchers to distinguish between the heat transfer that occurs at the water impingement point and in the falling film. They found that the peak heat flux in the water impingement point was 3×10^6 W/m^2 and occurred at a critical temperature of 150°C, however in the streaming zone the peak heat flux was much lower reaching only 1×10^6 W/m^2.

As modelling of the DC casting process became more sophisticated, it became apparent that there was a need to also model the stress state in the ingot so that phenomena such as butt curl and ingot cracking could be addressed. Initial attempts at this were done in a de-coupled manner so that the models were divided into two separate tasks; modelling of the thermal distribution in the ingot during solidification and modelling of the stress state in the ingot during and after casting, using the thermal distribution in the ingot as an input. More recently, there has been a trend to try and couple both the thermal and stress models as they have a strong influence on each other, especially during the problematic start-up phase, where the high thermal gradients cause large thermal stresses and strains to occur in the ingot as this in turn causes the ingot to macroscopically deform and alter the heat transfer.

Hannart et al. [23] were some of the first researchers to develop a fully coupled 3D thermal-stress model using the commercial FEM package MARC of the start-up phase for the DC casting process so that thermal strains during casting could be predicted. Fjaer and Jensen [24] also developed a fully coupled 3D model of the start-up phase and used it to assess the influence of the bottom block shape on the distortion of the butt of the ingot during casting. Mariaux et al. [25] developed a fully coupled 2D model to predict butt curl during the start-up phase of the electromagnetic (EM) casting process. Drezet et al. [7] developed a fully coupled 3D model of the start-up phase for DC casting using ABAQUS.

Many different numerical methods have been used to quantify the constitutive behaviour of the solid material during DC casting. Hannart et al. treated the solid phase as an elasto-viscoplastic, isotropic material, and used an empirical constitutive relationship as shown in Equation 2.6.

$$\bar{\sigma} = c(T)(\bar{\varepsilon}_p^* + \varepsilon_p^0)^{n(T)}\left(\dot{\bar{\varepsilon}}_p + \dot{\varepsilon}_p^0\right)^{m(T)} \qquad (2.6)$$

where $\bar{\sigma}$ is the equivalent flow stress, $\dot{\bar{\varepsilon}}_p$ is the equivalent plastic strain rate and $\bar{\varepsilon}_p^*$ is a hardening parameter, computed as the sum of plastic strain accumulated by the material at temperatures below 400°C. ε_p^0, $\dot{\varepsilon}_p^0$, c(T), m(T) and n(T) are coefficients which were determined based on tensile tests.

Drezet [26] considered the material in the solid state to exhibit steady state creep behaviour and conducted tensile creep experiments to determine the alloy dependent constants required in the Garofalo law to quantify this.

Moriceau [27] and Janin [28] used a temperature dependent elasto-plastic model to simulate the stress generation and to study the hot cracking tendencies for round aluminum billets. Matthew and Brody [29] similar to Drezet et al. introduced steady-state creep deformations into their analysis of the thermal stresses and Heinlein et al. [30] proposed a boundary element method to study transient temperature fields and associated stress fields in static solidifying bodies.

The most comprehensive modelling work done on the thermomechanical effects during DC casting was done by Fjaer and Mo [31]. These authors developed a finite element model ALSPEN, in which the thermally induced stresses and strains that develop during DC casting were calculated by a finite element method. In this model, the metal is described as an isotropic elastic-viscoplastic material with strongly temperature dependent properties. In their model both low temperature time-independent deformation and high temperature time-dependent deformation (i.e., creep) are considered.

More recently, Mo and Holm [32] have used constitutive equations with internal state variables in mathematical calculations of thermally induced strains and stresses in DC casting of aluminum billets. These constitutive equations relate the total viscoplastic strain rate to the stress, the temperature and some internal variables that represent the microstructural state of the material.

2.3 Summary

The key mechanical information required to accurately model the stresses and strains which develop in the ingot as it is being cast, is the characterization and quantification of the constitutive behaviour of the material being cast from the point at which it first begins to behave like a solid at high temperature down to room temperature.

Although there is a large number of studies in the literature related to the deformation of wrought aluminum alloys, these experiments have typically been done over temperature, strain rate and strain regimes which are quite different from those which the material is exposed to during casting.

As shown in the literature review, there appears to be some amount of uncertainty regarding the best approach to adopt to quantify the inelastic deformation occurring in the DC casting process. Throughout the literature it is evident that the approaches used fall into two main categories; an elastic time-independent plastic and elastic time-dependent creep due in part to the realization that both creep and plastic deformation are likely to occur to varying degrees over the entire temperature range experienced during DC casting process.

In order to optimize the casting parameters and consequently avoid cracking during solidification, two major tasks are required: 1) the development of a thermal-stress model capable of predicting the thermal and stress profiles of the material for any given casting recipe and 2) the characterization of the constitutive behaviour of the as-cast material during the DC casting process.

Chapter III - Scope and Objectives

3.1 Objectives

Direct Chill (DC) casting is one of the most important processes in the production of aluminum alloys. Some of the major problems encountered during casting of high strength aluminum alloys such as AA5182 and AA6111 are hot tears and cracks that occur during solidification and are caused by thermally induced stresses and strains. Successful casting of these high strength aluminum sheet ingots requires a more fundamental understanding of the material response in the mushy zone and solid state in order to predict the stresses and strains which occur during the DC casting process.

As a result, the objectives of this research project will be the following:

- to characterize as-cast AA5182 material behaviour under similar strain rate and temperature conditions as it is exposed to during DC casting in the solid state (i.e., $\dot{\varepsilon}$ = 1.0 - 1.0E-5 s^{-1} and T = 500-250°C

- to determine the best way to mathematically represent the constitutive behaviour in the solid state during DC casting using the constitutive models available within ABAQUS.

3.2 Methodology

The methodology employed in the execution of this research encompassed both experimental measurements using industrial as-cast aluminum samples as well as mathematical modelling of the experimental tests conducted.

For the experimental component of the program, the Gleeble1500[®‡] thermomechanical simulator was used. Compression and tension tests were conducted under a variety of temperatures (500-250°C) and strain rates (1.0E-5 - 1 s^{-1}) to reflect typical conditions the material would be exposed to during the DC casting operation at both the center and surface of the sheet ingot. The mathematical modelling was undertaken using the commercial Finite Element package ABAQUS.

3.2.1 Model validation

Model validation was performed by doing cyclical compression and tension tests with a hold time under load after each deformation using the Gleeble1500[®]. These tests reflected more accurately the type of stress history the material would be exposed to during DC casting. In order to test the model developed in ABAQUS, different temperatures and strain rates than those tested to develop the constitutive relationships were used.

Figure 3.1 shows schematically how the experimental, modeling and validation activities within the project were linked.

---

‡ Gleeble® is a registered trademark of Dynamic Systems Inc.

```
┌─────────────────────────────────────────────────────┐
│                    Experimental                     │
│                 Gleeble   1500 tests                │
│   •    T = 250 - 500°C and    $\dot{\varepsilon}$ =  1- 1E-5 s⁻¹ │
│                    • compression                    │
│                      • tension                      │
└─────────────────────────────────────────────────────┘
                           │
                           ▼
┌─────────────────────────────────────────────────────┐
│                     Modelling                       │
│            ABAQUS Deformation Model of              │
│                Gleeble   experiments                │
│    (creep, strain rate independent plasticity and strain │
│    rate dependent plasticity constitutive equations) │
└─────────────────────────────────────────────────────┘
                           │
                           ▼
┌─────────────────────────────────────────────────────┐
│                  Model Validation                   │
│                 Gleeble   1500 tests                │
│                      • cyclical                     │
└─────────────────────────────────────────────────────┘
```
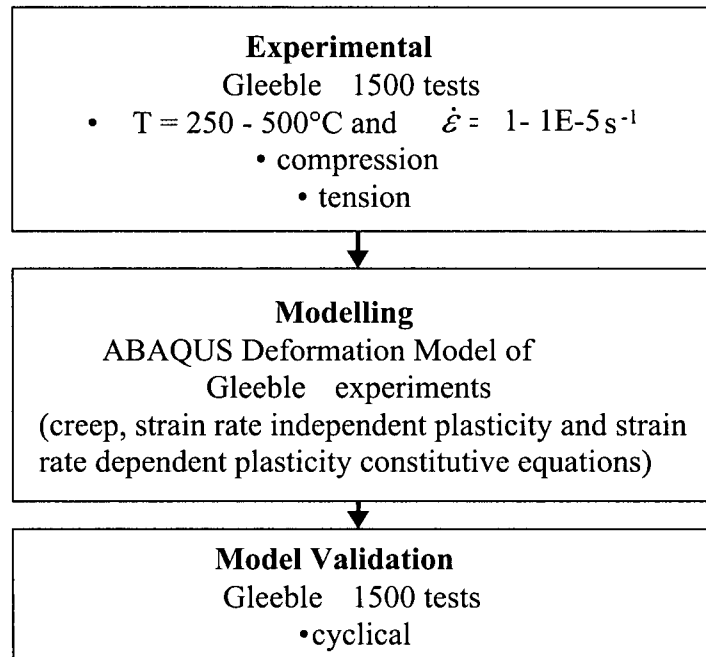
Figure 3.1 – Schematic of research methodology.

Chapter IV - Experimental

4.1 Start material

The experimental work was carried out on a commercially significant aluminum alloy AA5182 (Al-4.5%Mg) supplied in the as-cast form (after DC Casting) by Alcan International Arvida Laboratories. The chemical composition of the alloy is shown in Table 4.1

Table 4.1 – Composition of AA5182 used in this study.

Mg (%)	Si (%)	Cr (%)	Fe (%)	Cu (%)	Mn (%)	Ti (%)
4.66	0.06	0.002	0.21	0.057	0.31	0.023

As shown in Figure 4.1, the grain size of the ingot cast material varied significantly from the surface to the interior. As a result the material used for our experiments was taken close to the surface of the as-cast ingot and had a typical as-cast grain size of 1mm as shown in Figure 4.1. It is interesting to note that, this grain size is much larger than typical slab-gauge grain size of 81 μm for wrought AA5182 [33].
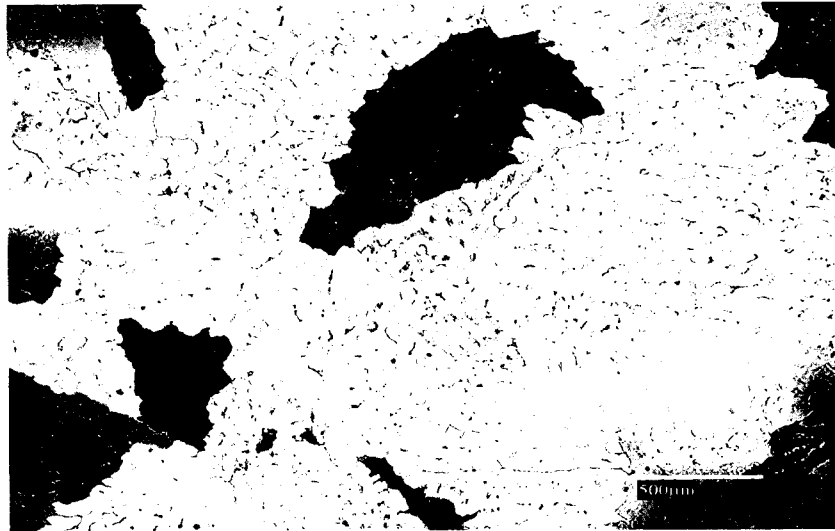
a) Close to surface
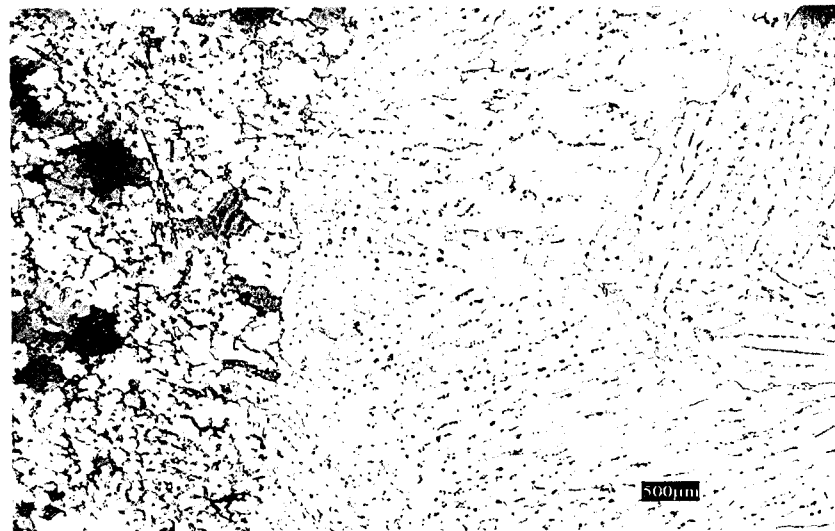
b) 5 cm from surface

Figure 4.1 – Starting as-cast AA5182 used for the experiments for: a) close to ingot surface and b) 5cm from ingot surface.

4.2 Deformation of as-cast samples

The experimental program was performed on a Gleeble1500® thermomechanical simulator which is capable of deforming a sample under extremely well controlled strain, strain rate and temperature conditions. Specimens of AA5182 were machined from as-cast sheet ingot stock and used for compression, tension and combination compression and tension tests.

4.2.1 Compression Tests

The axisymmetric compression test is one of the standard tests used for establishing the stress-strain response of a material at high temperatures. The major disadvantage of axisymmetric compression testing is barreling which occurs due to lateral friction restraint on the end faces. The resulting inhomogeneous deformation introduces errors in the computed stress values after a strain of approximately 0.7 has been reached [34,35].

Compression testing was conducted using the Gleeble1500® and cylindrical specimens of 10mm diameter x 15mm length were used. As shown in Figure 4.2, the test specimens were resistance heated at 10°C/s to test temperatures in the range 500-250°C, held at that temperature for one minute and then deformed to a true strain of 0.6 at nominal strain rates ranging from $1s^{-1}$ to 1.0E-5 s^{-1}. Stopping the tests at a true strain of 0.6 avoided the errors associated with barreling.
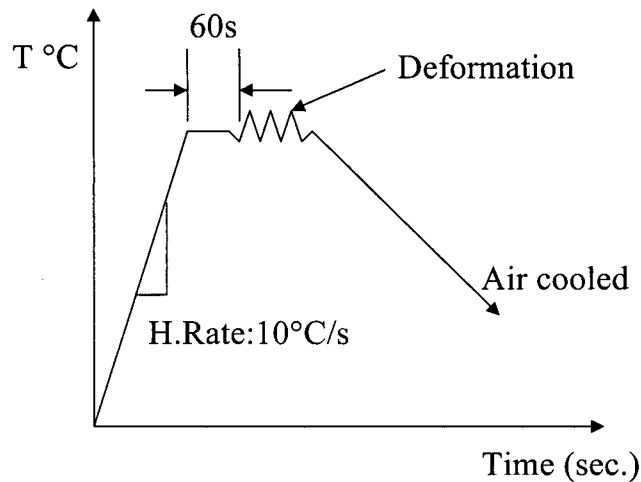
Figure 4.2 - Thermal/Deformation history of samples
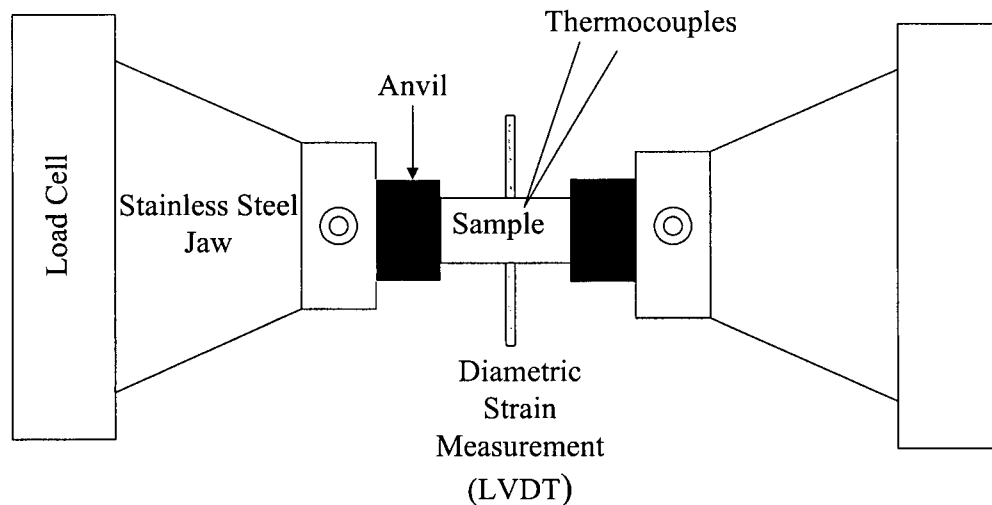
Figure 4.3 – Schematic of the compression test conditions on the Gleeble.

Referring to Figure 4.3, the sample temperature, during a test, was measured using a chromel-alumel thermocouple of 0.6mm diameter wire which was spot-welded on the surface of the sample. A clip-on, quartz rod, diametric Linear Variable Differential Transducer (LVDT), were mounted across the diameter of the test sample at the mid-span of the specimen to measure the diametric strain (C-Strain) during testing. Similarly, another LVDT was also mounted to measure the change in length during hot deformation

24

(L-strain). The compression tests were performed using constant ram velocity and the *mean* strain rate at each test temperature was calculated.

A total of twenty compression tests were run and the test conditions chosen were based on typical strain rate and temperatures experienced by the material in the solid state during DC casting. Table 4.2 shows the experimental test matrix used for the compression tests. The actual temperature, strain rate and total strain achieved during each test were evaluated from the measured data and used in the data analysis and are shown in Appendix C Table C.1.

Table 4.2. Experimental test matrix for compression tests.

Temperature (°C)	Strain rate (s^{-1})
300 400 500	1.0E-5
300 350 400 450 500	1.0E-3
250 300 350 400 450 500	1.0E-1
250 300 350 400 450 500	1.0E1

Flow stress and strain values were calculated from the raw Gleeble data using an Excel spreadsheet which converted the load and displacement measured to a flow stress and strain. A full description of this procedure is given in Appendix A.

4.2.2. Tension test

A total of eleven tensile tests were run to compare the material response under tension to that under compression. Similar to the compression tests, a thermocouple was

26

spot-welded on to the sample so that the temperature could be controlled during deformation. The displacement was measured using the L-strain LVDT. The tensile samples had a gauge length of 27mm and a gauge diameter of 5mm, Appendix A shows a schematic of a tensile test specimen and Table 4.3 shows the experimental test matrix used for the tensile specimens.

Table 4.3 Experimental matrix for tension tests.

Temperature (°C)	Strain rate (s⁻¹)
300	1.0E-2
400	
300	
400	1.0E-1
500	
250	
300	
350	1.0E1
400	
450	
500	

Appendix C Table C.2 summarizes the actual temperatures and strain rates used for each test and the resulting measured steady-state flow stress.

4.2.3 Combination compression-tension tests

In order to validate the constitutive equations developed, a total of eight cyclical stress tests were run on the Gleeble1500 which consisted of initially loading the sample in compression, under a given strain rate to a fixed strain, holding it at this strain for 120 seconds, while the stresses in the sample relaxed, and then reloading the sample in tension at the same strain rate to the same amount of strain and holding it for 120 seconds to allow the stresses in the sample to relax. The entire cycle was then repeated. The combined compression/tension samples had a gauge length of 17mm and a gauge diameter of 6 mm. These dimensions were slightly different from those used for the tensile tests to avoid buckling in the sample during the deformation. Table 4.4 shows the experimental test matrix used for the cyclical specimens. Appendix A Figure A1.3 shows a schematic of the samples used for these tests and the corresponding measured strain rates, temperatures and strains under each cycle.

Table 4.4 Experimental matrix for combination (compression/tension) tests.

Temperature (°C)	Strain rate (s^{-1})
375	
475	1.0E-5
375	
475	1.0E-4
375	
475	1.0E-3
375	
475	1.0E-1

Chapter V - Mathematical Modelling

The Gleeble tests performed (i.e., compression, tension and combination compression and tension) for the experimental part of the project as well as the material response during the deformation were simulated by developing a mathematical model using the commercial FEM package, ABAQUS™. ABAQUS is a comprehensive, general-purpose finite element analysis package that can be used to simulate the thermal and stress state that exists in a material under a given set of conditions.

The reason the ABAQUS commercial FEM package was chosen to simulate the material constitutive behaviour during the experiments was because it is the commercial FEM package we have chosen to develop a 3D thermal-stress model of the DC casting process and we wanted to examine the various methods available within the package to model material constitutive behaviour.

5.1 Simulation of constitutive behaviour in ABAQUS

Various constitutive models are available in ABAQUS to simulate a wide range of material behaviour subject to loading. From a numerical viewpoint the constitutive model within ABAQUS is used to quantify the state of stress at a material integration point given the state of strain [36].

The mechanical constitutive models provided in ABAQUS consider both the elastic and inelastic response. The inelastic response of the material can be modeled using either strain rate-dependent or strain rate-independent inelastic models and can be defined with a yield surface (plastic) or without a yield surface (creep).

In modelling the overall deformation that occurs and the resulting stress and strain state, the general assumption within ABAQUS is that the total deformation is made up of elastic and inelastic components, and in the case of a thermal stress analysis, a thermal strain. The various sources of strain are assumed to be additive according to Equation 5.1.

$$\varepsilon_{total} = \varepsilon_{el} + \varepsilon_{pl} + \varepsilon_{creep} + \varepsilon_{thermal} \tag{5.1}$$

where ε_{total} is the total strain, ε_{el} is the elastic strain, ε_{pl} is the plastic strain, ε_{creep} is the creep strain and $\varepsilon_{thermal}$ is the thermal strain. A similar expression exists in terms of strain rate. Both the strain and strain rate at a given load depend on the response of the material given by the constitutive law.

5.1.1 Elastic deformation

In modelling the elastic response of a material subject to a load, various models are available in ABAQUS, the simplest of which is linear elasticity where the stress is proportional to the strain as shown in Equation 5.2:

$$\sigma = D_{el} : \varepsilon_{el} \tag{5.2}$$

where D_{el} is a matrix that may depend on temperature but generally does not depend on the deformation except in the case of a non-linear elastic material. This method of modelling the elastic response of the material can be used for simulating the material response during the Gleeble experiments as the elastic strains in the tests conducted are very small compared to the inelastic strains.

5.1.2 Inelastic deformation

ABAQUS contains a number of different constitutive models to describe the inelastic behaviour of a material during deformation. These models can be strain rate-dependent (viscoplasticity or creep) or strain rate-independent (plasticity). The various plasticity models require the definition of a yield surface that may or may not evolve with deformation.

In the simplest plasticity model within ABAQUS, the yield stress does not change as a function of strain rate. In the case where one yield stress is defined at each temperature in a tabular format, the material is said to be "perfectly plastic". Variations of the plasticity model available within ABAQUS also allow isotropic hardening as well as non-isotropic hardening to be handled.

Within ABAQUS, strain rate-dependent inelastic deformation can be handled using either the strain rate-dependent plasticity option or the creep option. In the strain rate-dependent option, ABAQUS uses direct tabular data in which the test data is provided as tables of yield stress values versus equivalent plastic strains at different equivalent plastic strain rates and temperatures. The yield stress at a given strain, strain rate and temperature is then interpolated directly from these tables.

Alternatively, strain rate dependent inelastic deformation can be handled within ABAQUS by using simple built-in creep laws such as power law creep, shown in Equation 5.3 or Garofalo creep shown in Equation 5.4 to simulate the material behaviour during deformation.

$$\dot{\varepsilon}_{cr} = A \tilde{q}^{n} \, t^{m} \qquad (5.3)$$

31

where;

$\dot{\bar{\varepsilon}}_{cr}$ is the uniaxial equivalent creep strain rate

$\tilde{q}$ is the uniaxial equivalent deviatoric stress (i.e., the Von Mises equivalent stress)

t is the total time, and

A, n and m are defined by the user as functions of temperature.

The power law model of creep is attractive in terms of its simplicity, however as shown in the literature review this model is generally used to model the steady state flow stress under low stress conditions and under-predicts the steady state flow stress under high stress conditions

Within ABAQUS, Garofalo or the hyperbolic-sine creep law is modeled using the following equation:

$$\dot{\bar{\varepsilon}}_{cr} = A(\sinh B\tilde{q})^n \exp\left(-\frac{\Delta H}{R(\theta - \theta^Z)}\right) \qquad (5.4)$$

where

$\dot{\bar{\varepsilon}}_{cr}$ and $\tilde{q}$ are defined above

θ is the temperature

θ^Z is the user-defined value of absolute zero on the temperature scale used

ΔH is the activation energy

R is the universal gas constant

A, B and n are other material properties.

It is important to point out that these standard creep laws are used for modelling secondary or steady state creep. For more complicated cases of creep there is also the ability to input a user defined creep routine to simulate the material behaviour.

If creep and plasticity occur simultaneously and implicit creep integration is in effect, both behaviours may interact and a coupled system of constitutive equations needs to be solved.

5.2 Simulation of Gleeble experiments using ABAQUS

As previously stated, the rational for developing an ABAQUS based FE model was to examine the suitability of the various material constitutive models available. The model requires specification of the sample geometry, boundary conditions (including the nature of the loading) and the material response (constitutive behaviour).

5.2.1 Geometry

The model developed in ABAQUS to simulate the Gleeble experiments was a 2-D axisymmetric model. As shown in Figure 5.1, the whole cylinder was modeled and due to circumferential symmetry it yielded a domain with a height of 15mm and a radius of 5mm. The finite element mesh consisted of 40 2-D 4-noded isoparametric axisymmetric elements, and had a total of 55 nodes. ABAQUS evaluates the material response at each material integration point of which there are 4 located at the nodal positions.
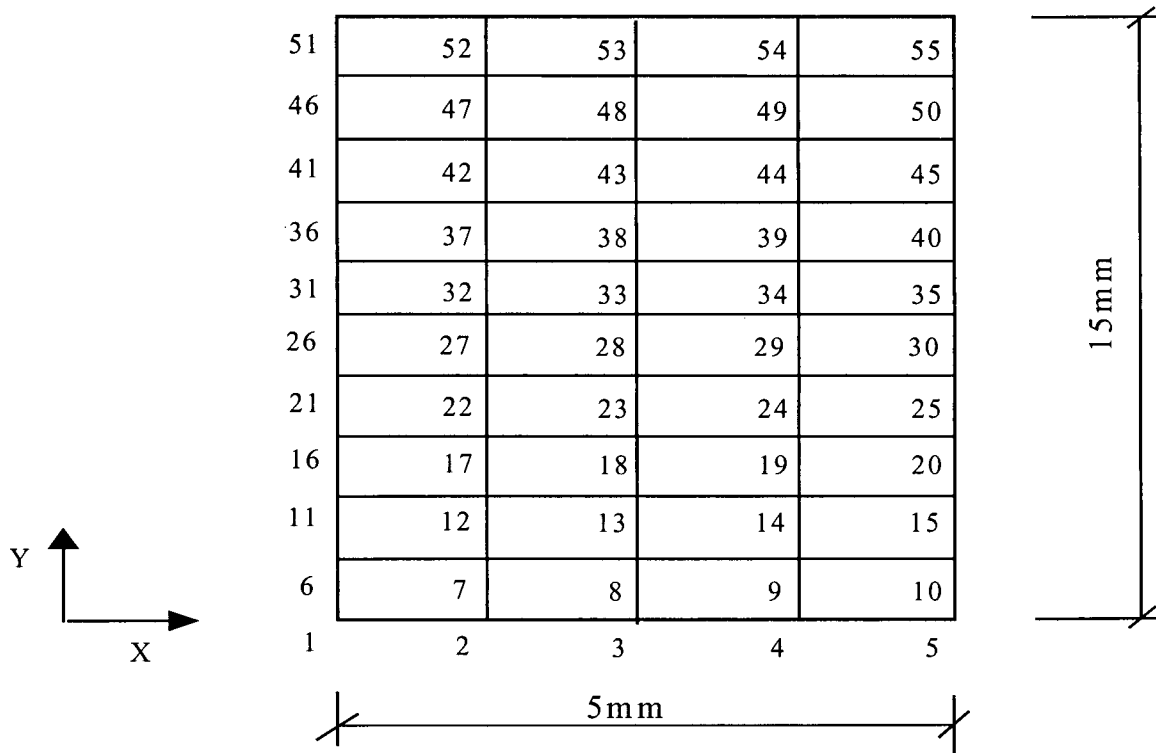
Figure 5.1 Finite element mesh (2-D) of compression sample for stress analysis.

5.2.2 Boundary conditions

The boundary conditions applied to the domain employed for the 2-D stress model are illustrated in Figure 5.2. Due to symmetry, displacement at the center of the sample in the radial direction (i.e., at x = 0) is constrained. At the bottom of the sample (i.e., y = 0) displacement in the axial-direction is set to zero so as to avoid rigid body motion. In Figure 5.2 displacement in the axial direction is represented by "V" and displacement in the radial direction is represented by "U".

34
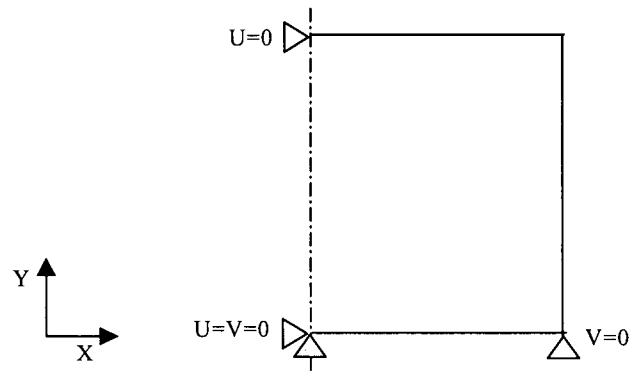
Figure 5.2. Displacement-based boundary conditions on the test specimen.

The samples in the experiments were subject to a fixed displacement rate in order to examine their response to increasing load.

The deformation of the samples in the experiments is simulated in ABAQUS by defining an amplitude curve in the input deck. An amplitude curve allows arbitrary time (or frequency) variations of load, displacement, and other prescribed variables to be given throughout a step (load step) or throughout the analysis (using total time). In order to simulate a given experiment, the total displacement, time to achieve the total displacement and temperature were defined in the ABAQUS input deck. Figures 5.3 illustrate a typical strain-time response during uniaxial compression testing.
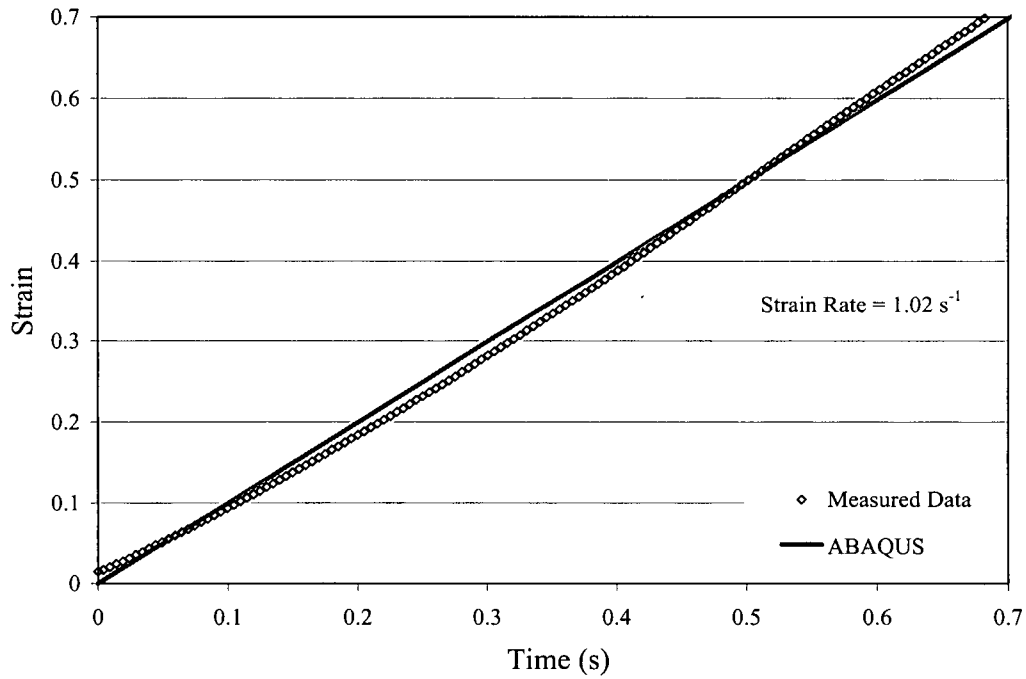
Figure 5.3. Model predicted strain-time response as compared to experimental measurements (compression test T = 253°C, $\dot{\varepsilon}$ = 1.0 s⁻¹ and total ε = 0.7).

5.2.3 Material properties

As previously described the material properties required by ABAQUS to describe the deformation at elevated temperature include the elastic as well as the plastic properties, or the elastic as well as the creep properties depending on the approach to be adopted.

The parameters required to describe the elastic component of the deformation model include the Young's modulus and Poisson's ratio. The Young's modulus was determined from the literature [37] and was input as a function of temperature. These

values are shown in Appendix D in Table D.24. A constant value of Poisson's ratio of 0.3 was used in the analysis.

Data for both the strain rate independent plasticity and strain rate dependent plasticity models is input into ABAQUS in the form of a table. In the case of the strain rate independent plasticity the data includes the yield stress, equivalent plastic strain at that stress and the temperature at which the data applies. For the strain rate dependent plasticity model, the table of data must also include the strain rate at which the data applies. In addition, the strain rate dependent plasticity algorithm also requires the so-called "static" flow stress, or the stress at an associated equivalent plastic strain rate approaching zero. Tabular data of the plasticity properties of the material under varying temperature and strain rate conditions used in ABAQUS was based on the compression tests performed and is given in Appendix D in Tables D.1-23. For strain rate independent plasticity model values at a strain rate of 1.0E-3 s^{-1} were used.

The classical metal creep behaviour in ABAQUS can be defined in several forms by providing the required parameters appropriate for the creep law. These can either be isotropic creep or anisotropic creep models and require that the material elastic properties as discussed earlier be defined in each case.

Chapter VI - Results and Discussion

6.1 Experimental results

The results of the experimental tests conducted on as-cast AA5182 aluminum alloy presented in this chapter include the uniaxial compression tests, uniaxial tension tests and combination uniaxial compression/tension tests. A comparison between the thermomechanical properties of wrought material obtained from literature and the experimental results of as-cast AA5182 alloy is also presented.

6.1.1 Compression test results

Under the conditions present in the DC casting process the material is subject to a range of temperatures and strain rates.

Experimental measurements from uniaxial compression tests indicated that the deformation temperature has a significant influence on the measured flow stress for as-cast AA5182 alloy. As seen in Figure 6.1 and in an expanded plot Figure 6.2, the amount of work hardening that occurs and steady state flow stress increases with decreasing temperature at a constant strain rate.
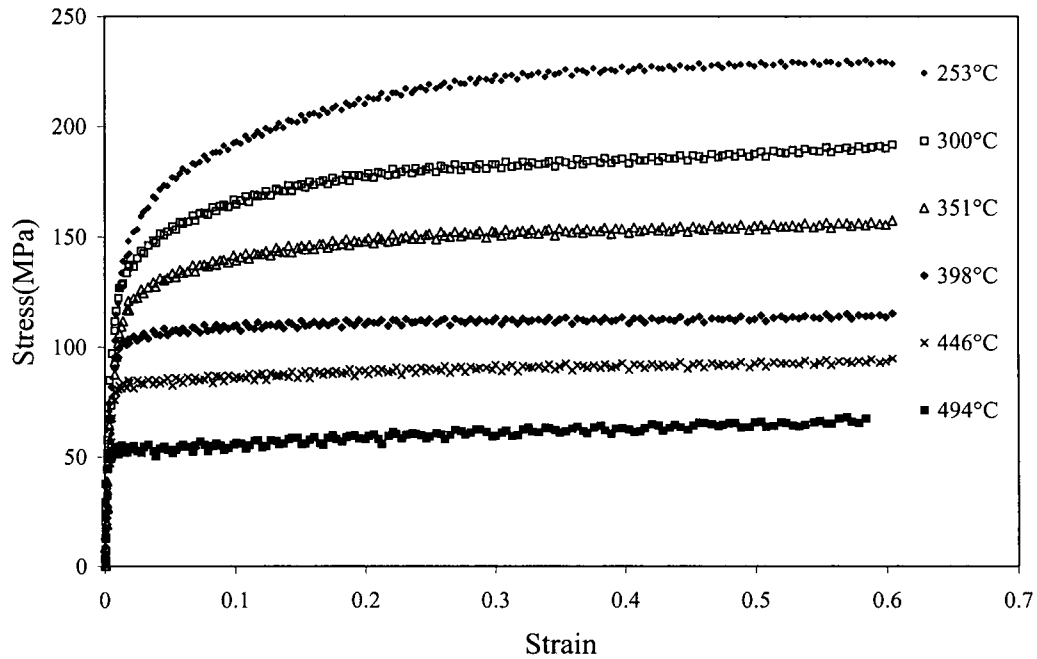
Figure 6.1 - Effect of temperature on the measured stress strain curves in compression for as-cast AA5182 alloy ($\dot{\varepsilon}_{mean} = 1.0s^{-1}$).

As the temperature increases the ability of dislocations to cross-slip and climb is enhanced and hence the flow stress required to effect the deformation and the amount of work hardening which occurs decreases. It can also be seen from Figure 6.2 that stress strain curves measured below ~350°C exhibit strain hardening to a much higher level of strain than stress strain curves measured above ~350°C. A similar trend was evident at other strain rates tested.
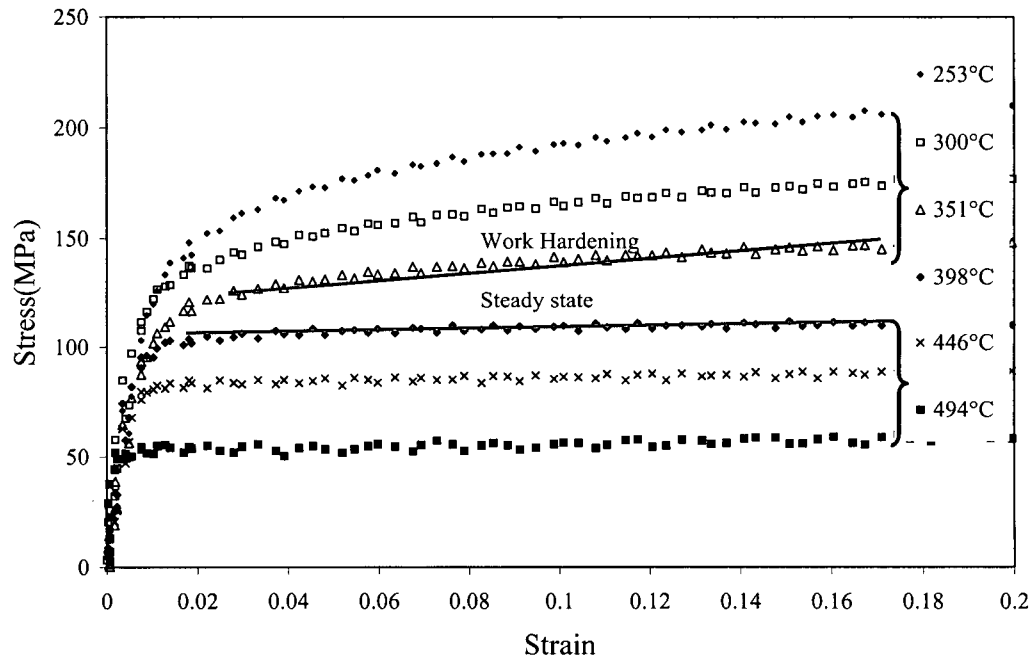
Figure 6.2 - Steady state and work hardening conditions during compression tests

for AA5182 alloy at constant strain rate ($\dot{\varepsilon}_{mean}$ = 1.0 s^{-1}).

As shown in Figure 6.3 the material behaviour is also very sensitive to the applied strain rate, with the flow stress increasing as the applied strain rate increases, with the difference in steady state flow stress being ~145MPa for a change in strain rate from 1.0E-5 s^{-1} to 1 s^{-1} at 300°C.
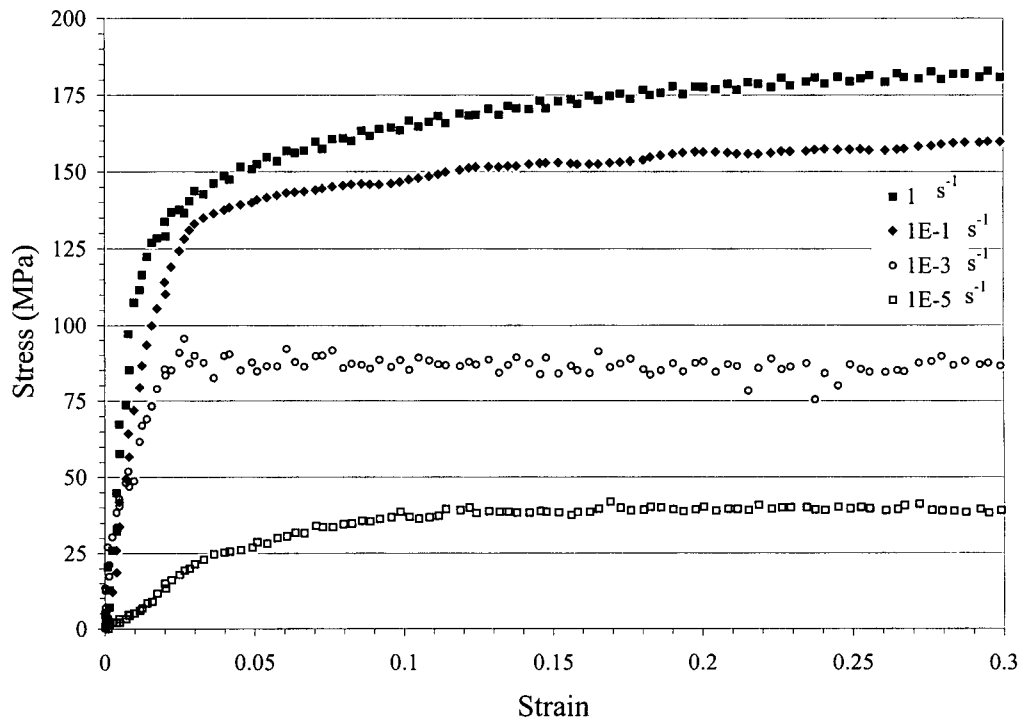
Figure 6.3 - Effect of strain rate on the measured flow stress strain curves in compression

for as-cast AA5182 (T_{def} = 300°C).

6.1.2 Tension tests

Tension tests were also conducted on the start material to determine if the material response was similar in both tension and compression.

Experimental results obtained from tension tests also showed the strong sensitivity of the material behaviour to temperature. Figure 6.4 shows the effect of temperature during deformation at constant strain rate. Again it was observed that the flow stress increases with decreasing temperature at constant strain rate. During the uniaxial tension tests a decrease in the flow stress was also evident once the material started to neck, hence these tests were limited to low total strains.
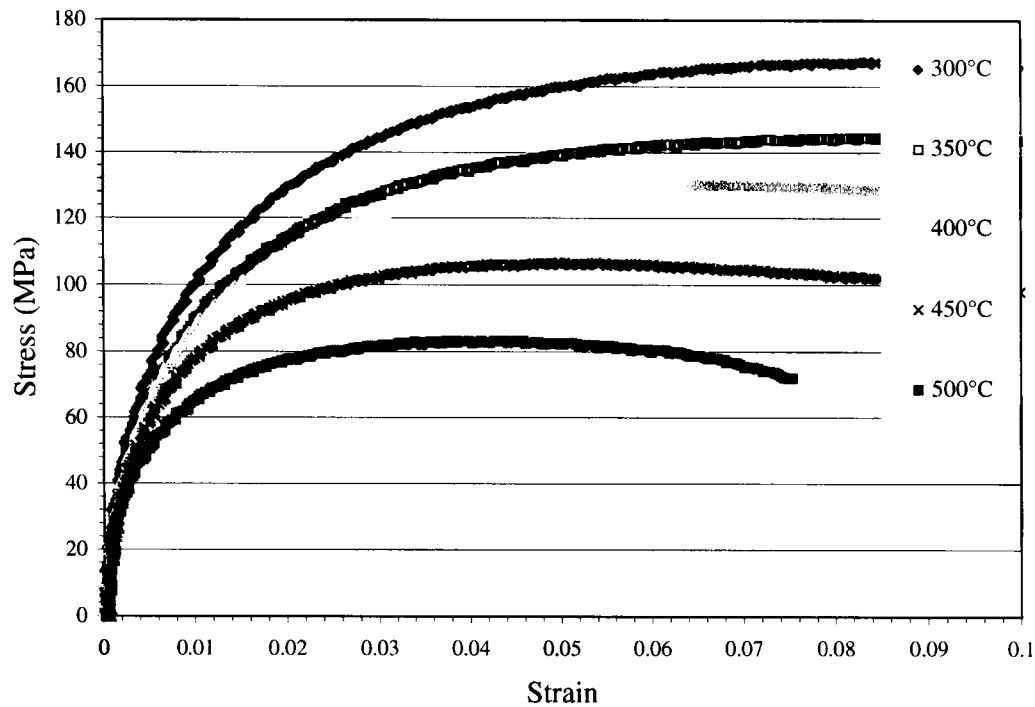
Figure 6.4 - Effect of temperature on the measured stress strain curves for as-cast

AA5182 alloy in tension ($\dot{\varepsilon} = 1.0s^{-1}$).

The effect of strain rate in tension has also been investigated at constant temperature and results show that the response of the material is also sensitive to strain rate. It was observed that the flow stress increases with strain rate at constant deformation temperature, as was the case for the uniaxial compression tests. At the temperature of about 500°C and at a strain of 0.6 necking occurred in the tensile sample as shown in Figure 6.4 with the flow stress beginning to drop.

As shown in Figures 6.5, comparison of the material behaviour in both tension and compression, show that within experimental error, the measured stress strain behaviour was similar, therefore the material response is independent of the deformation path. However, as can be seen the material tested in tension consistently exhibited a slightly lower steady state flow stress than the material tested in compression.
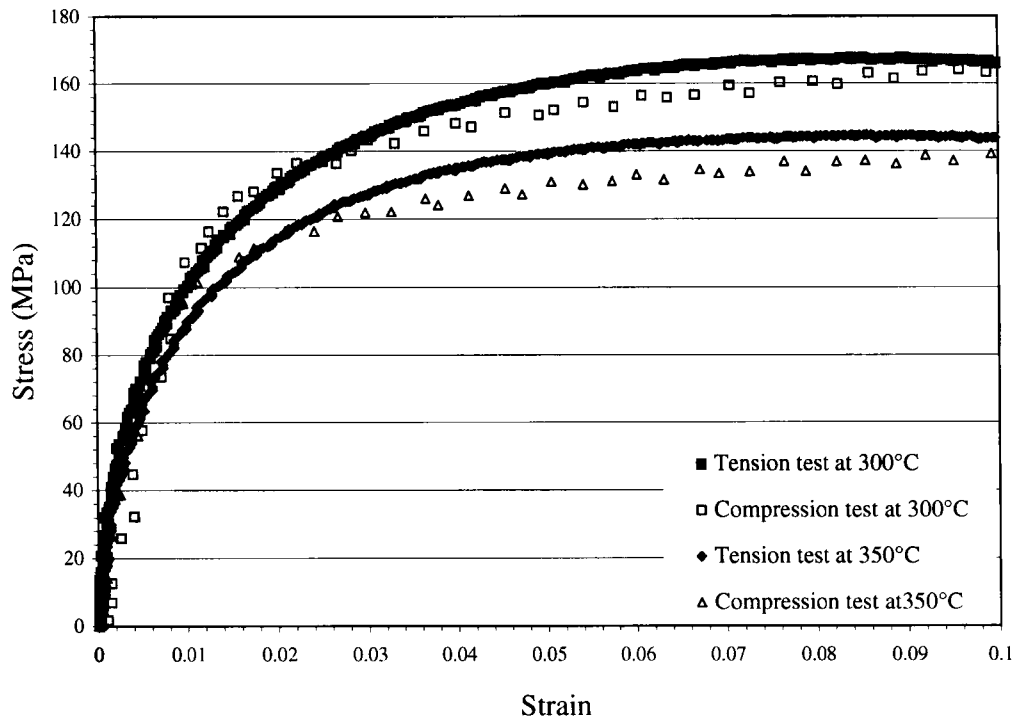
Figure 6.5 - Comparison of tension and compression results for as-cast AA5182

$$(\dot{\varepsilon}_{mean} = 1.0 \text{ s}^{-1}).$$

6.1.2 Cyclical tests

During DC casting of aluminum sheet ingots, the thermal stresses and strains generated are the result of the complex thermal history experienced by the ingot as it solidifies and cools to room temperature. Preliminary thermal stress analyses indicate that at the center of the ingot the cooling rates are relatively slow (i.e., <0.01°C/s) whereas at the surface the cooling rates are much faster (i.e. >1°C/s) [38].

An illustration of the cyclical stress state experienced by the ingot as it cools is shown in Figure 6.6 using predictions from an uncoupled thermal-stress model of the start-up phase of the DC casting process for aluminum. In this model the material is

treated as an elastic-plastic material with temperature dependence but no strain rate dependence. Since the material behaviour is simplified and does not include strain rate dependence the prediction shown in Figure 6.6 will likely contain some errors and stress relaxation of the material will not occur.
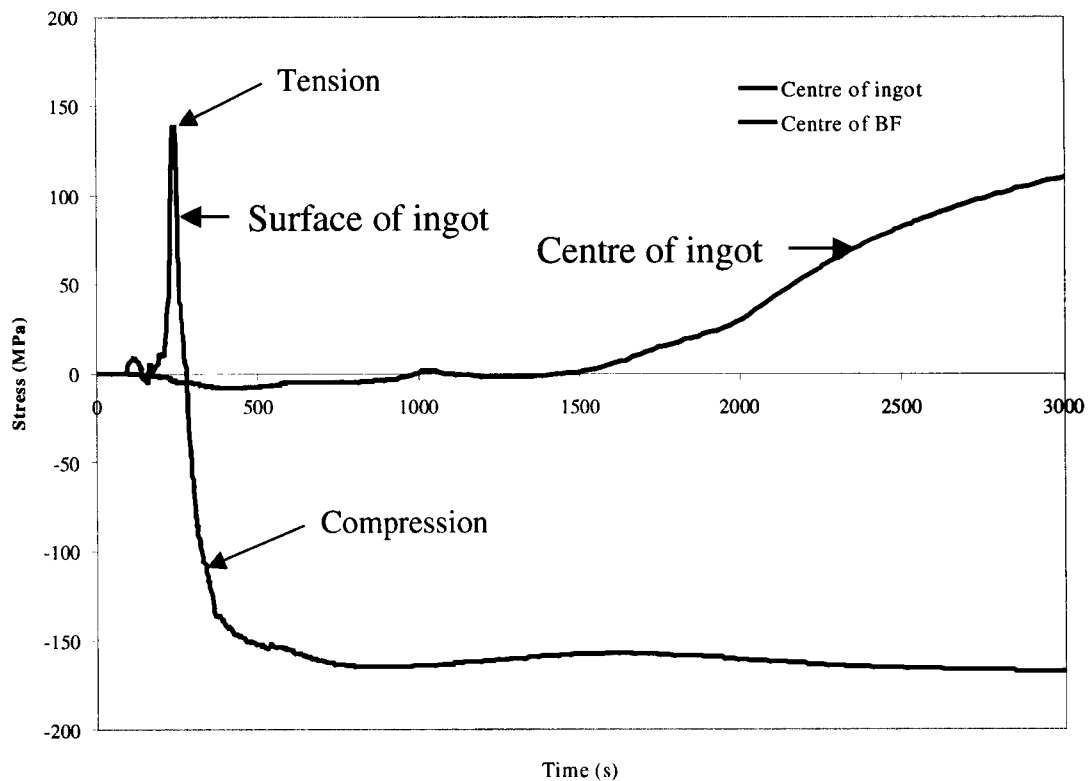
Figure 6.6 - Predicted stress evolution at various positions in a sheet ingot as it cools to room temperature [38].

In the DC casting process, the surface of the solidifying ingot initially is in a state of tension and is thermally contracting at a high rate. The stress state then changes to compression as the ingot continues to cool and the temperature gradient moderates.

In contrast, at the center of the solidifying ingot, the material initially is in a state of compression and this gradually changes into a state of tension. Compared to the ingot surface the cooling rates are relatively low.

To simulate the cyclical nature of the stresses experienced by the material as it cools during DC casting and, to validate the constitutive equations developed, we conducted cyclical loading tests using the Gleeble1500 which consisted in initially loading the test specimen in compression to a prescribed strain at a prescribed strain rate and holding for 120s to allow stress relaxation to occur. The sample was then reloaded at the same strain rate in tension to the same strain as during compression and held again to allow stress relaxation to occur. The cyclical tests were performed under different temperatures and strain rates than those used for the compression and tension tests so that the constitutive models within ABAQUS could be validated. Figures 6.7 and 6.8 are classical illustrations of the material response under the cyclical loading tests for different temperatures.
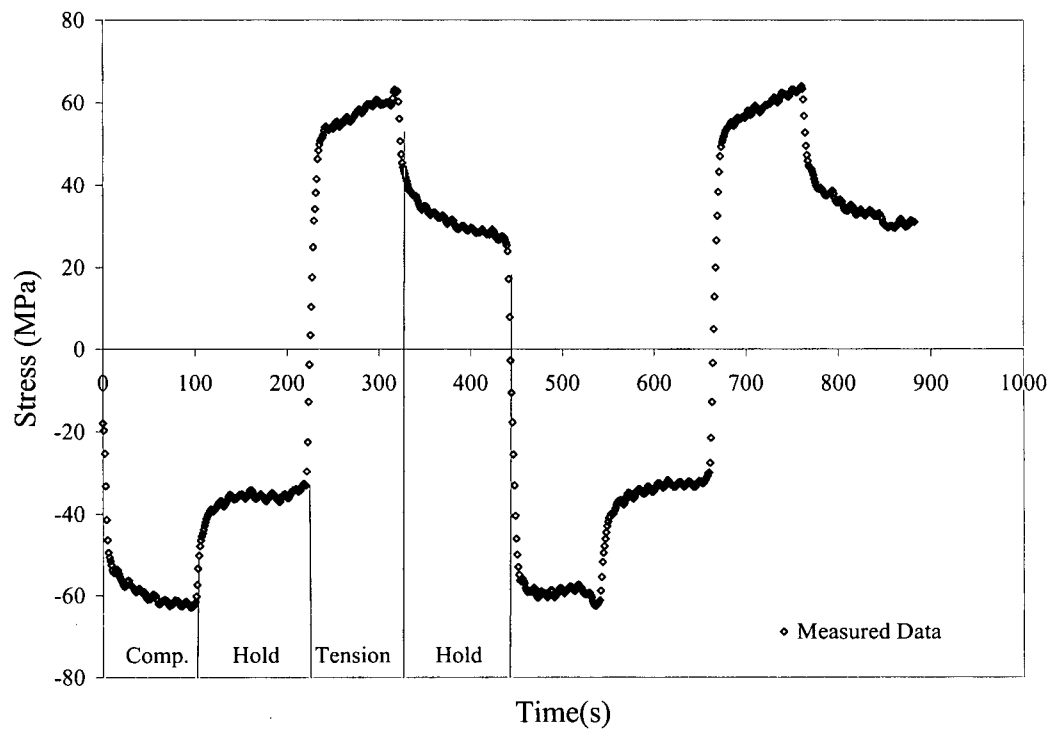
Figure 6.7. - Cyclical loading at temperature of 367°C and nominal applied

strain rate of 1.5E-3 s^{-1}.
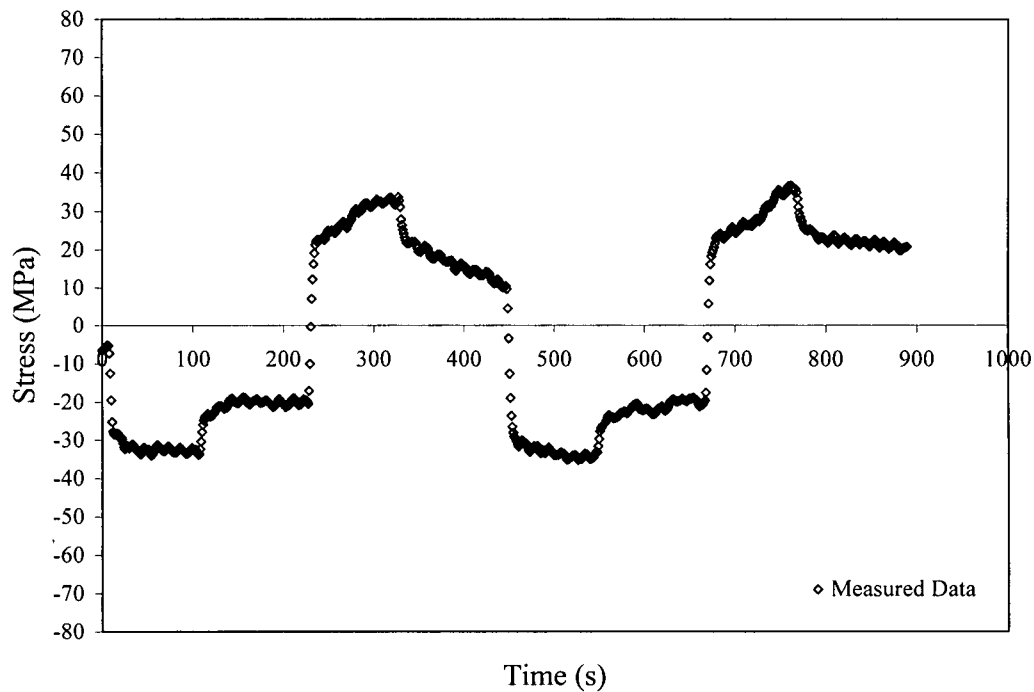
Figure 6.8. - Cyclical loading at temperature of 468°C and nominal applied

strain rate of 1.5E-3 s^{-1}.

As shown in these Figures during uniaxial compression, the material exhibits elastic deformation followed by inelastic deformation which includes some work hardening prior to the development of the steady state flow stress. After compression, the material is held at temperature and during this period the strain rate decreases and the material relaxes. The material is then reloaded in tension and again exhibits elastic deformation followed by inelastic deformation. After tension, the material is again held at temperature and during this period the strain rate decreases and the material relaxes. This entire cycle was then repeated.

Some asymmetry between the compression and tension portions of the cyclical tests was observed. This could be due in part to residual strain in the specimen during the

tension/compression cycle and hold – i.e., the strain does not go back to zero during tension.

An examination of the measured strain history as shown in Figure 6.9 confirmed this and shows some residual straining in the specimen during the tension cycles. Consequently, the measured steady state stress during loading in tension was slightly higher than that measured in compression.
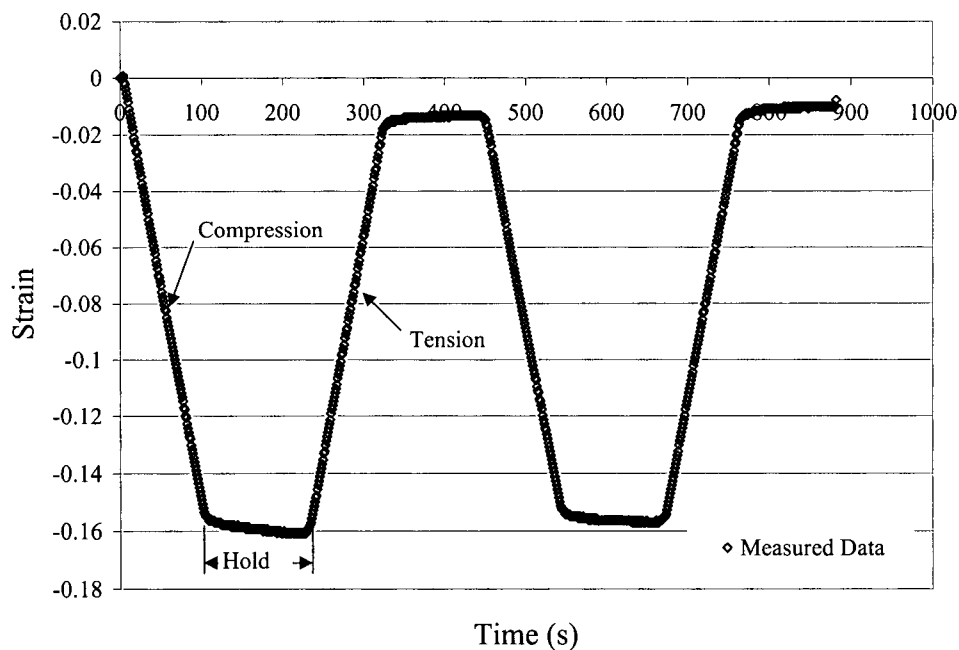
Figure 6.9- Strain history of as-cast AA5182 during cyclical loading (T_{def} = 367°C, $\dot{\varepsilon}$ = 1.0E-3 s^{-1} and ε = 0.15).

6.1.3 Difference between as-cast and wrought material

A comparison of the experimental data for as-cast AA5182 to wrought data found in the literature [19] indicates that the difference in constitutive behaviour between as-

48

cast and wrought material at different temperatures appears insignificant. Figure 6.10 shows a comparison between the measured as-cast AA5182 stress-strain curve as compared to that found in the literature for a wrought AA5182 alloy. Clearly this observation is in contrast to, one observed by Lu and co-workers for AA7050 alloy. This may be due to the fact that our starting material is a non-heat treatable alloy and the only difference in the structures would be the grain size and size and distribution of the constituent particles. Further, these results suggest that the experimental procedures used in this investigation are sound.
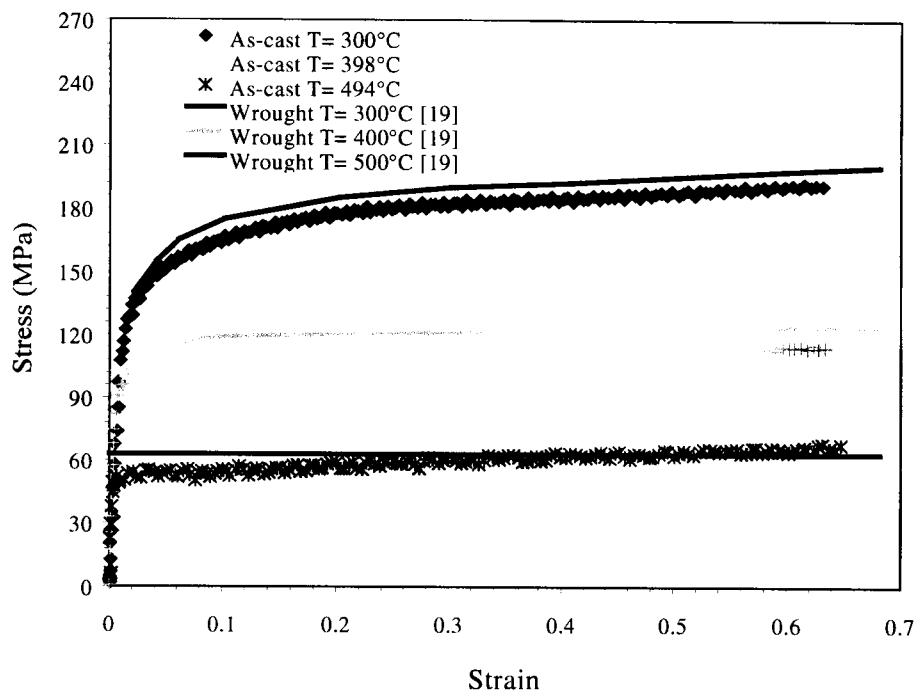
Figure 6.10. Comparison between wrought and as-cast AA5182 alloy at strain rate of 1.0 s^{-1}.

6.2 Constitutive model development

As previously discussed, there are a variety of constitutive models in ABAQUS to model the inelastic behaviour of materials subject to high temperature deformation. Model simulations for each set of tests have been performed in ABAQUS employing three types of constitutive models; creep, strain rate independent plasticity and strain rate dependent plasticity in order to ascertain which of these models would be better suited to mathematically represent the constitutive behaviour of as-cast AA5182 alloy subject to the range of temperatures and strain rates experienced in the DC casting process.

6.2.1 Creep model

Using steady state flow stress data measured from the compression tests of as-cast AA5182; three standard creep equations were developed as shown in Table 6.1 and evaluated for their suitability. Steady state flow stress was defined as the stress where a subsequent increase in strain produced less than 0.5 MPa difference

Constants for the hyperbolic sine in the constitutive equation were determined by developing a simple program which iteratively solved for the constants required to minimize the difference between the measured and predicted values. Constants in the power law and the exponential equations were determined graphically as shown in Appendix E.

An activation energy of 126 kJ/mole (Q_{def}) was assumed for the stress analysis.

Table 6.1 – Creep based equations developed for as-cast AA5182.

Creep Equation	Equation Developed from Data
Power law	$\dot{\varepsilon} = 1.65x10^{12}\, \sigma_s^{11.95} \exp\left(-\dfrac{Q_{def}}{RT_{def}}\right)$
Exponential law	$\dot{\varepsilon} = 4.16x10^{6} \exp(0.058\sigma_s) \exp\left(-\dfrac{Q_{def}}{RT_{def}}\right)$
Hyperbolic sine	$\dot{\varepsilon} = 2.9x10^{11} [\sinh(0.005\sigma_s)]^{6.74} \exp\left(-\dfrac{Q_{def}}{RT_{def}}\right)$

Appendix E gives a detailed description of how the constants were determined in each of the creep equations.

Although the physical significance of the constants are not clearly defined, Jonas et al. [39] consider the A values to be a structure factor at high stress levels (i.e. proportional to the density of activateable sites). Figure 6.11 shows the fit of the developed equations to the experimental data by plotting the dependence of the steady state flow stress on the value of Z (the Zener-Hollomon parameter where $Z = \dot{\varepsilon}\exp\left(\dfrac{Q_{def}}{RT_{def}}\right)$). As shown, at low values of Z, the results are consistent with the power-law relation whereas at higher Z values the curves approach the exponential relation. Figure 6.11 also indicates the ability of the hyperbolic sine relationship to represent the experimental data under a wide range of strain rate and temperature conditions.
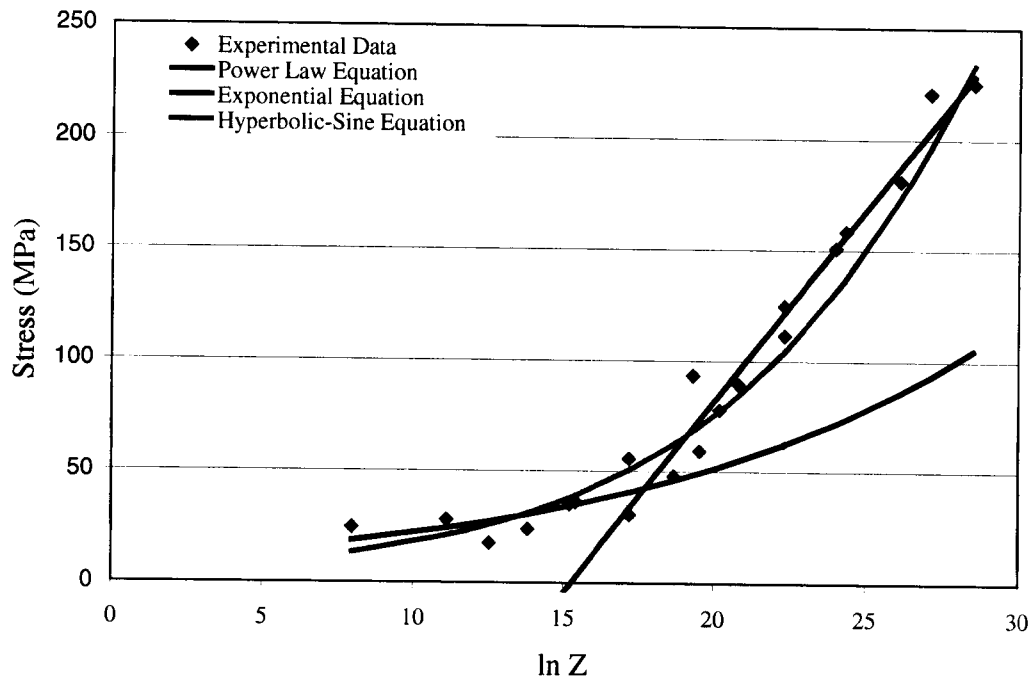
Figure 6.11 - Dependence of flow stress on the instantaneous values of Zener-Hollomon parameter Z.

Traditionally, high temperature deformations of materials have been modelled using creep with secondary or steady state creep equations being applied in models of the DC casting of aluminum alloys as well as hot rolling and extrusion models.

Modelling creep behaviour of the material in ABAQUS was done using a hyperbolic sine law with creep constants A, n, and m developed as previously described, defined in the input deck with no dependencies

6.2.1 Strain rate independent plasticity model

The strain rate independent plasticity deformation model in ABAQUS was also used to simulate the material behaviour within the range of experiments conducted at the

various temperatures. It uses a tabular data input from the measured stress strain curves. As discussed earlier in chapter five, the tabular data chosen for this model was obtained from experiments conducted at a strain rate of 1.0E-3 s^{-1} as this is the mid way point in the range of strain rates over which the entire tests were performed to represent an average of the data obtained.

In this model the deformation of the material is assumed to be isotropic and elastic-plastic with only the effect of temperature on the flow stress. Within the temperature bounds ABAQUS linearly interpolates to solve for the stresses and outside these bounds it assumes that the model is temperature invariant. Table D1.1 in Appendix D shows the data employed in the strain rate independent plasticity model simulations.

6.2.2 Strain rate dependent plasticity model

As in the case of the strain rate independent plasticity model, the strain rate dependent plasticity model also uses tabular data as input but also includes the material's sensitivity to strain rate during deformation. The data therefore spans the complete range of strain rates and temperatures under which the stress strain curves were determined. The material deformation is assumed to be isotropic elastic-plastic with strain rate dependence. An added variable required in the input deck for this model is the so-called "static flow stress".

Static flow stress was determined for as-cast AA5182 alloy at various temperatures by deforming the material to a predetermined strain at a constant strain rate and then holding it at this strain for a period of time to allow the stress to relax as the strain rate decreased. Figure 6.12 is an illustration of the stress, strain and strain rate evolution as a function of time during a test. As can be seen from the Figure after the

deformation is complete the strain rate decreases and approaches a value of zero. During this period, as the strain rate decreases, the measured stress relaxes to a lower value. As shown in the Figure, even after the strain rate has essentially reached a value of zero, the stress continues to decrease slightly. Referring to Figure 6.13, the amount of relaxation the stress undergoes is a function of the deformation conditions as well as the hold time and the temperature. For the purpose of modelling, the static flow stress was assumed to be equal to the average value of stress attained during relaxation from 2 to 9 seconds.
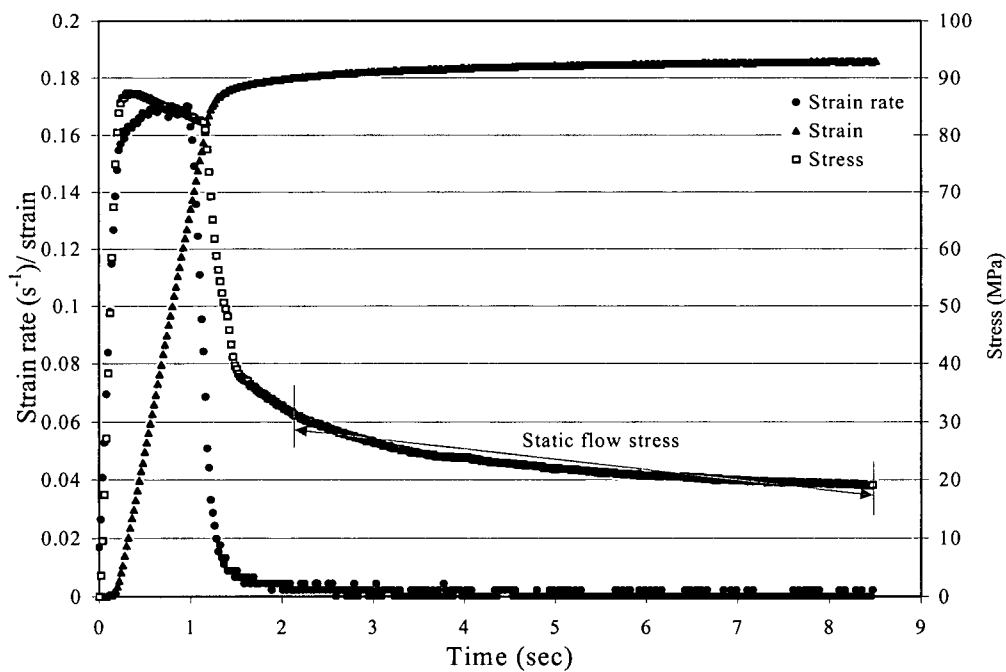
Figure 6.12 - Determination of static flow stress ($T_{def/hold} = 402°C$, $\dot{\varepsilon} = 0.17\ s^{-1}$, $\varepsilon = 0.18$, $t_{hold} = 8.5s$).
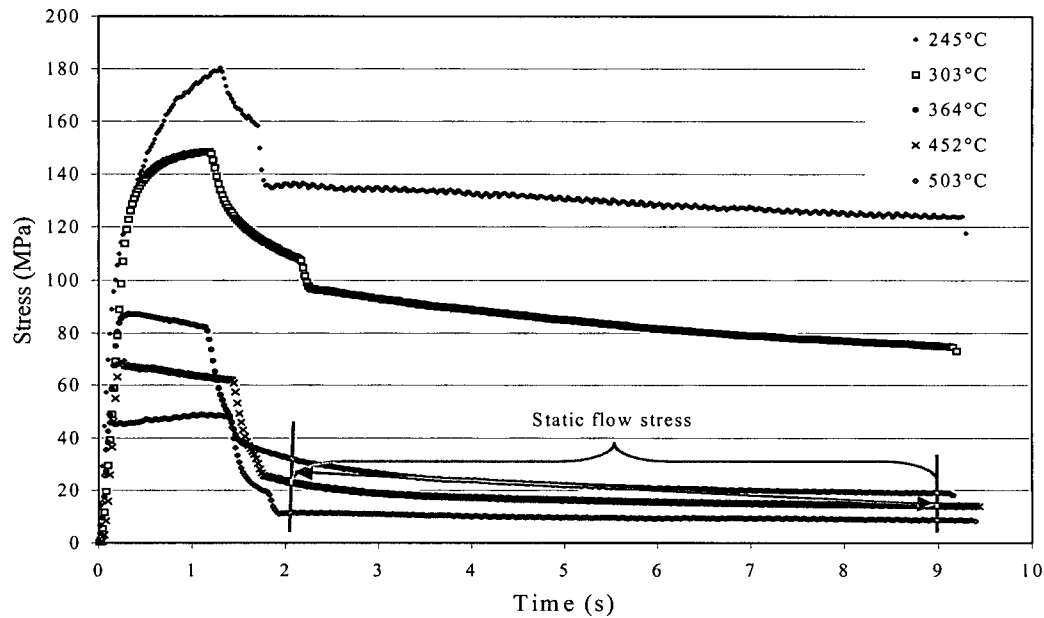
Figure 6.13 - Temperature dependence of static flow stress of as-cast AA5182 at strain rate of 1.7E-1 s^{-1}.

6.3 Model validation

The models developed were tested against cyclical loading data obtained outside the bounds of the experimental data used to develop the constitutive models to examine their robustness.

6.3.1 Cyclical loading tests

To ensure the ABAQUS model was simulating similar deformation experienced by the sample during the experiments, a comparison between the applied strain-time behaviour was made against the experimental measurements. As shown in Figure 6.14, the ABAQUS model simulates ideal experimental conditions, with the strain returning to zero during the tension cycles. These conditions were not seen during the experiments

but, a comparison of the strain rates between the experiments and the ABAQUS model indicate they are very similar.
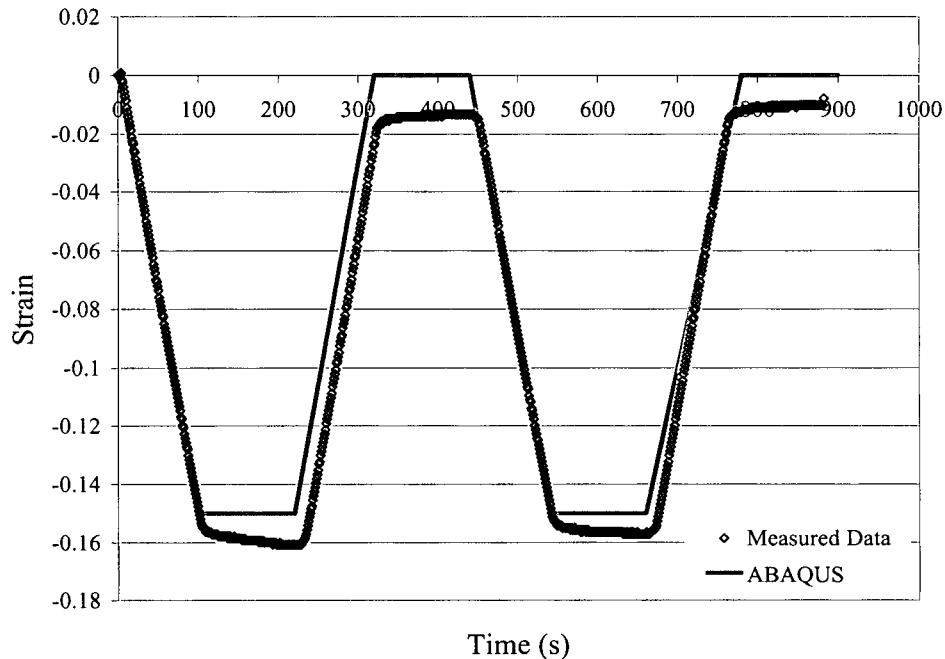
Figure 6.14 - Model predicted strain-time response as compared to experimental measurements (cyclical test at T = 367°C, $\dot{\varepsilon}$ = 1.5E-3 s^{-1} and ε = 0.15).

6.3.2 Creep model validation

The results for the creep model in ABAQUS show that even though the value of the constants derived from the development of constitutive models were based on monotonic uniaxial tests, it is able to reproduce the material's behaviour under cyclical loading conditions including a hold. The major disadvantage of the creep model however, is that it fails to capture the strain hardening in the material during loading at low temperatures. It is observed from Figure 6.15 that the creep model predicts the steady state flow stress reasonably well for the conditions tested. However, it over predicts the

relaxation of the material during the holding period. For high temperature conditions (i.e., > 350°C), the creep model is able to represent the stress strain behaviour of the material reasonably well. Under low temperature conditions the creep model is not adequate as it fails to capture work hardening of the material. In addition, Garofalo's creep model is for secondary creep where the creep rate is constant. During DC casting the inelastic strains experienced by the material are low (i.e., < 0.05) and a primary creep model where the creep rate changes during straining is more appropriate.
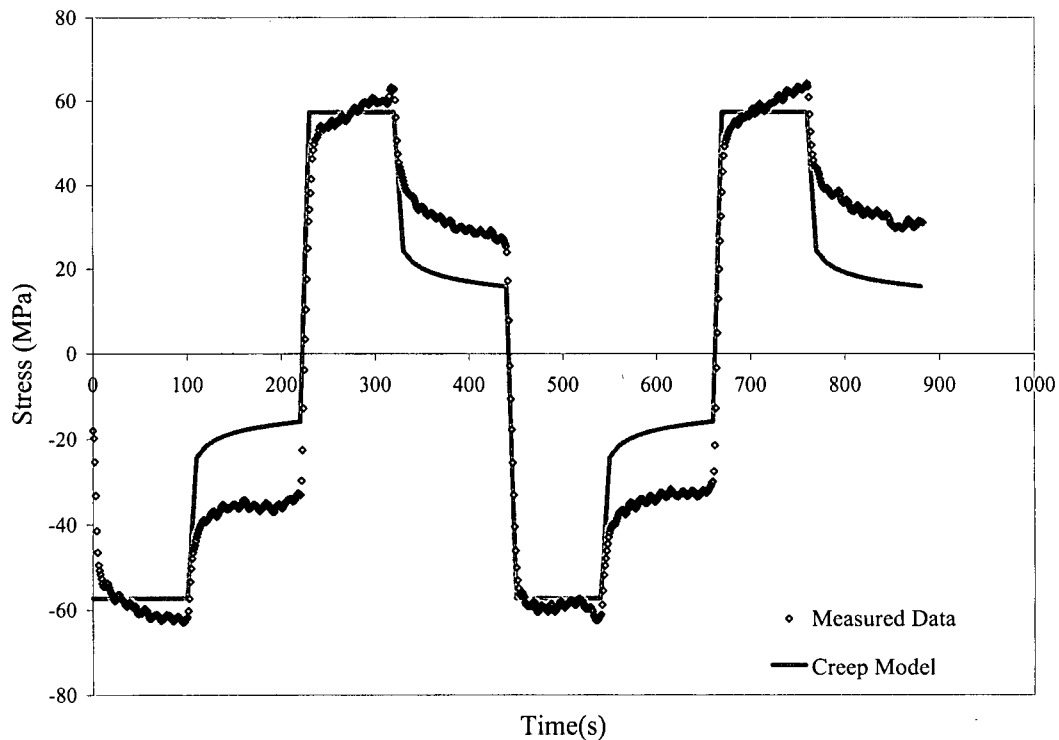
Figure 6.15 - Creep model validation during cyclical loading at constant strain rate of 1.5E-3 s^{-1} and temperature of 367°C.

6.3.3 Strain rate independent model validation

From Figure 6.16 it is evident that the strain rate independent plasticity model is able to reasonably predict the flow stress of the material during deformation. However, it

is unable to reproduce the stress relaxation during holding. In addition, the strain rate independent plasticity model will be unable to accurately predict the flow stress of the material during deformation under strain rate conditions significantly different from $1.0E{-}3$ s^{-1}.
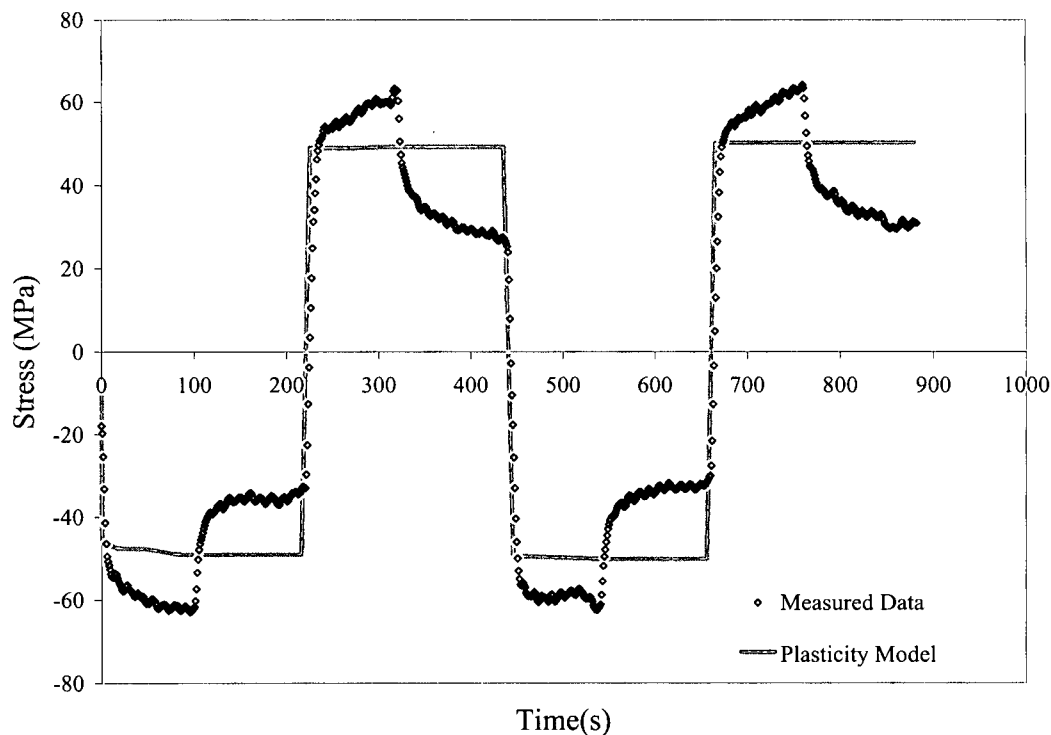
Figure 6.16 – Strain rate independent plasticity model validation during cyclical loading at strain rate of $1.5E{-}3$ s^{-1} and temperature of 367°C.

6.3.4 Strain rate dependent plasticity model validation

As shown in Figure 6.17, cyclical loading simulations in ABAQUS using the strain rate dependent plasticity deformation model shows reasonable agreement with experimental measurements. This model was able to represent the material behaviour during the deformation as well as the hold period. As shown in Figure 6.16 and 6.17, the prediction of the flow stress during the loading portion of the cycle is not as good for the

strain rate dependent and independent plasticity models used in ABAQUS as that using the creep model. The reason is because ABAQUS uses a linear interpolation technique to estimate the influence of temperature on the flow stress when using tabular data for the strain rate dependent and independent models whereas the creep model includes the more realistic exponential dependence on temperature.
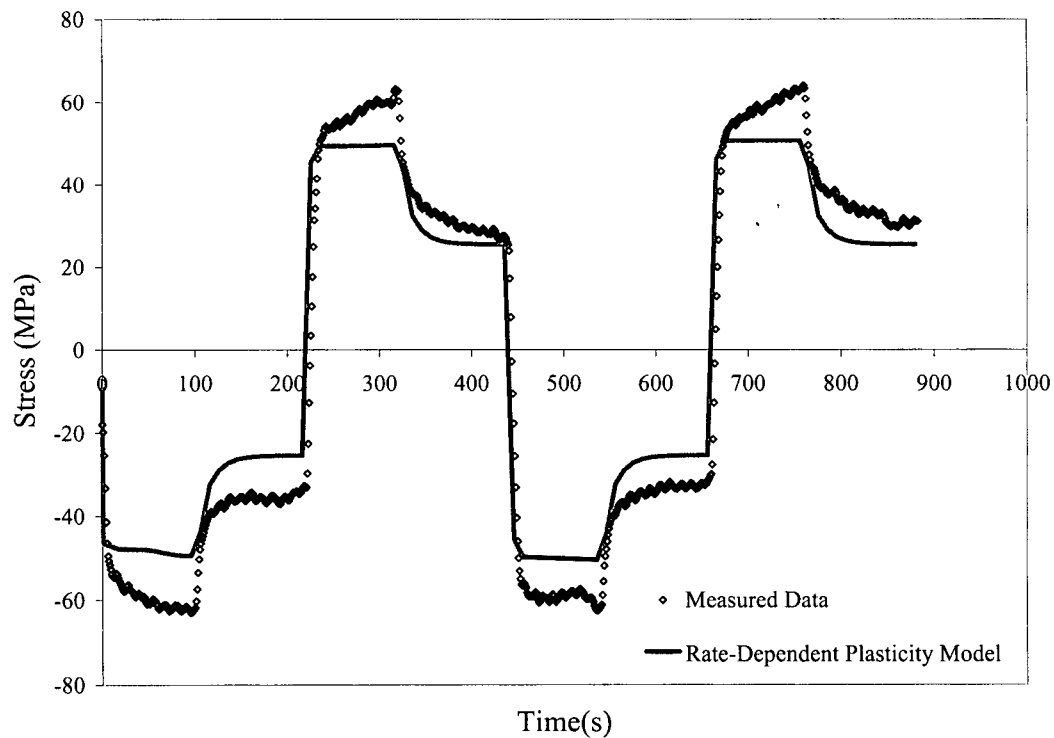
Figure 6.17 – Strain rate dependent plasticity model validation during cyclical loading at strain rate of 1.5E-3 s^{-1} and temperature of 367°C.

As shown in Figure 6.18, the advantage of the strain rate dependent plasticity model over the creep model is that at low temperatures it is capable of reproducing the strain hardening behaviour of the material.
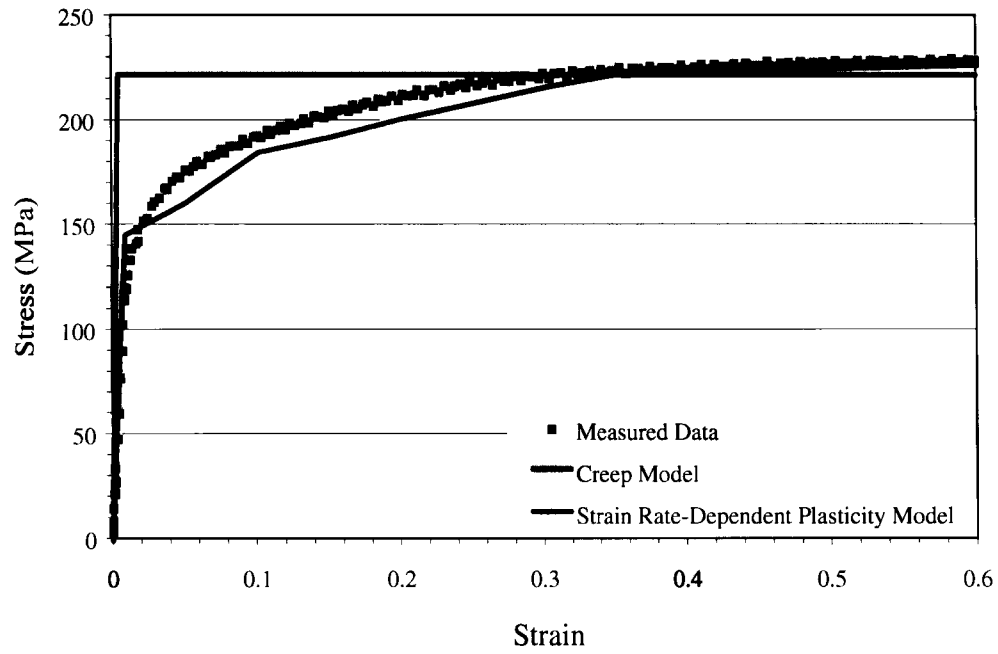
Figure 6.18. – Comparison of creep model and strain rate dependent plasticity model to

uniaxial compression test at $T_{def} = 253°C$ and $\dot{\varepsilon}_{mean} = 1.0$ s^{-1}.

Chapter VII - Summary and Conclusions

7.1 Summary and conclusions

A number of high temperature uniaxial compression and tensile tests and cyclical compression/tension tests have been performed on the Gleeble1500 thermomechanical simulator and the flow stress for an AA5182 alloy in the as-cast condition has been measured. The mechanical tests were performed on standard compression and tension samples at temperatures and strain rates similar to those experienced in the sheet ingot Direct Chill (DC) casting process, thus, at conditions relevant for thermally induced deformations in the DC casting process.

A commercial finite element (FE) software package ABAQUS has been employed to simulate the Gleeble deformation tests using a two-dimensional (2-D) axisymmetric model. The simulations were conducted to compare the various methods available within ABAQUS to simulate inelastic deformation.

To model the high temperature inelastic behaviour of the alloy within ABAQUS, three approaches were used, namely: steady state creep using Garofalo's law, strain rate independent plasticity and strain rate dependent plasticity. The parameters required for Garofalo's equation for steady-state creep were determined using a program in excel which minimized the error between the computed and experimentally measured steady state flow stresses. For the plasticity models, tabular data was developed for the variation in stress as a function of strain for each temperature and strain rate tested. The results of each of these models were then compared with the experimentally measured stress-strain curves.

Experimental results show that at temperatures up to ~350°C, some work hardening occurred. Above this temperature, very little work hardening occurred and steady-state flow stress was reached at much lower strains.

Comparison of the constitutive behaviour of as-cast AA5182 to wrought material show that the strength difference between the two at all temperatures is relatively insignificant. This similarity in the constitutive behaviour between as-cast and wrought AA5182 could be attributed in part, to the fact that at high temperatures the grain size does not significantly impact on the strength on the material and Al-Mg binary alloys do not show appreciable precipitation-hardening characteristics at magnesium concentration below 7%.

Simulations of the Gleeble experiments in ABAQUS indicate that the elastic creep model is capable of predicting the steady state flow stress and its dependence on the temperature and strain rate of the deformation. This model is also able to represent the stress relaxation that occurs in the material during the hold period of the cyclical test. The major disadvantage of this method, however, is its inability to capture the initial work hardening at lower temperatures. In addition, this creep law simulates secondary steady state creep where the inelastic strains are relatively high. In the DC casting process the inelastic strains are much lower and a primary creep model in which the creep rate decreased as the straining occurred would be more suitable. As a result, this method of modelling the material constitutive behaviour is more suitable for large deformations (i.e., $\varepsilon > 0.2$) and high temperatures (i.e., deformation temperature > 300°C).

The elastic strain rate-independent plastic model is able to capture the temperature dependence of the flow stress during deformation but does not account for strain rate

dependence. As a result, it was unable to simulate the stress relaxation in the material during the hold period of the cyclical test. This model is not suitable to simulate inelastic behaviour during DC casting as it does not capture the strain rate dependence of the material.

The elastic strain rate-dependent plastic model simulations indicated that the model was able to accurately predict the flow stress at low temperatures where there is substantial work hardening as well as at higher temperatures were strain hardening is not as prevalent. It was also able to capture the stress relaxation which occurred in the material during the hold period of the cyclical test. Consequently, this method of modelling inelastic deformation during DC casting within ABAQUS is the most suitable.

7.2 Recommendations

The constitutive model which should be used to model the material behaviour during the DC casting process in the solid state is the elastic strain rate-dependent plastic model. The following points summarize the reasons for this recommendation:

- There is very strong strain rate dependence to the material behaviour, especially at high temperatures.

- Plastic strains experienced by the material during DC casting are very low (e.g. < 0.05 inelastic strain) and correspond to the primary creep phase. The hyperbolic sine creep law describes secondary or steady state creep and will therefore over-predict the stresses at lower strain values associated with primary creep.

- Work hardening occurs at lower temperatures (i.e., < 300°C) and this stress-strain dependence cannot be captured using the hyperbolic sine creep law.

There is an exponential dependence of the flow stress with temperature, hence it is critical to ensure that when tabular data is used to model the inelastic deformation the temperature increments used are sufficiently small so that linear interpolation can adequately represent the exponential influence of temperature.

Once the elastic strain rate-dependent plastic model is integrated into the 3D thermal stress model it should be used to help design experiments which more closely reflect the temperature, strain and strain rate conditions experienced by the material in the solid state.

A load cell with much lower capabilities should be used on the Gleeble1500 so that high temperature and low strain rate tests can be conducted.

7.3 Scope for Future Work

Measurements and modelling of the material behaviour in the mushy zone i.e. 632-537°C would also be required if the material constitutive behaviour is to be fully obtained from the coherency temperature until the alloy fully solidifies.

References

1. E. F. Emley, "Continuous Casting of Aluminum", International Metals Review, 1976, pp. 75-115.

2. H. Fjaer and E.K. Jensen, "Mathematical Modelling of Butt Curl Deformation of Sheet Ingots. Comparison with Experimental Results for Different Starter Block Shapes", Light Metals 1995, Ed. J. Evans, TMS 1995, pp. 951-959.

3. Y. Caron and A. Larouche, "Importance of Understanding Ingot Butt Cooling Conditions at Start-Up: A Case Study", Light Metals 1996, pp. 963-969.

4. Thermomechanical Analysis of the DC Casting Start-Up Phase for Aluminum Sheet Ingots. October-December 2000. Report.

5. Solidification Characteristics of Aluminum Alloys. Vol. 3: Dendrite Coherency Ed. Susan P. Thomas AFS 1996, pp. 55-60.

6. Private Communication Joydeep Sengupta, December 1999.

7. J-M. Drezet and M. Rappaz, " Modelling of Ingot Distortions During Direct Chill Casting of Aluminum Alloys" Metallurgical Transactions A Vol. 27A 1996, pp. 3214-3224.

8. M. G. Chu and D. A. Granger, "The tensile Strength and Fracture behaviour of Partially Solidified Aluminum Alloys", Materials Science Forum Vol. 217(2222) 1996, pp. 1505-1510.

9. P. Ackermann and W. Kurz, "In-Situ Tensile Testing of Solidifying Aluminum and Al-Mg Shells " Materials Science and Engineering Vol. 75 1985, pp. 75-86.

10. O. Branswyck, J. Collot, P. Vicente-Hernandez, A-M. Chaze, and C. Levaillant," Investigation of Semi-Solid State Behaviour of Alloys Aimed at Process Modelling", Institute of Materials (UK) 1992, pp. 124-130.

11. W. D. Callister Jr." Materials Science and Engineering: An Introduction" John Wiley & Sons, Fourth Ed. 1997, pp. 220-222.

12. F. Garofalo, "An Empirical Relation Defining The Stress Dependence of Minimum Creep Rate in Metals", Metals Transactions. TMS-AIME, Vol. 227 1963, pp. 351.

13. Aerospace Structural Metals Handbook Vol. 3, Ed. W. F. Brown, Jnr., H. Mindlin, and C. Y. Ho, CINDAS/ Purdue University, 1995.

14. ASM Metals Hanbook, Vol. 2 10th Edition, ASM International, 1990.

15. Alloy Digest, Alloy Digest Inc., 1990.

16. H-M. Lu and H-Min, "Constitutive Modelling of High Strength Aluminum Casting", Light Metals 1997, Ed. R. Huglen, TMS 1997, pp. 1091-1095.

17. J. Barry Wiskel, "Thermal Analysis of the Start-Up Phase for the DC Casting of An AA5182 Aluminum Ingot", Ph.D. Thesis, UBC Vancouver Canada 1995, pp.196.

18. E. Herba and H. J. McQueen, "High Temperature Deformation of AA6061 with Comparison to AA6201 Alloy", Intl. Symposium on Hot Workability of Steel and Light Alloys-Composites CIM 996, pp. 53-60.

19. S .R. Chen, M. G. Stout, U. F. Kocks, S. R. MacEwen and A. J. Beaudoin, " Constitutive Modelling of AA5182 Aluminum As a Function of Strain Rate and Temperature", Hot Deformation of Aluminum Alloys II, Ed. T. R Bieler, L. A. Lalli, and S.R MacEwen, TMS 1998, pp. 205-215.

20. D. A. Peel and A. E. Pengelly," Mathematical Models in Metallurgical Process Development", Iron and Steel Institute 123, London 1970, pp.186-196.

21. D. C. Weckman and P. Niessen, "A Numerical Simulation of the D.C Casting Process Including Nucleate Boiling Heat Transfer", Metallurgical Transactions B 1982, Vol. 13B, pp.593-602.

22. Y. Watanabe and N. Hayashi, " 3-D Solidification Analysis of the Initial State of the DC Casting Process", Light Metals 1996, Ed. W. Hale, TMS 1996, pp.979-984.

23. B. Hannart, F. Cialti and R.V. Schwalkwijk, " Thermal Stresses in D.C. Casting of Aluminum Slabs: Application of a Finite Element Model",Light Metals 1994, Ed. U Mannweiler, TMS 1994, pp. 879-887.

24. H. G. Fjaer and E. K Jensen, "Mathematical Modelling of the Butt Curl Deformation of Sheet Ingots, Comparison with Experimental Results for Different Starter Block Shapes". Light Metals Ed. J. Evans TMS 1995, pp. 951-959.

25. S. Mariaux. M. Rappaz, Y Krahenbuhl and M Plata "Modelling of Thermomechanical Effects During the Start-Up Phase of the Electromagnetic Casting Process", Light Metals 1992, pp. 175-187.

26. J-M Drezet, "Direct Chill Casting and Electromagnetic casting of aluminum allloys: Thermomechanical Effects and Solidification Aspects". Ph. D. Thesis No 1509, EPFL, Lausanne, 1996.

27. J. Moriceau, " Thermal Stresses in Continuous D.C. Casting of Aluminum Alloys", Light Metals 1975, Vol. 2, AIME 1975, 119-133.

28. B. Janin "State of the Art of Computer Simulation of casting and Solidification Processes", Ed. H. Fredriksson, France 1986, pp. 305.

29. J. Mathew and H.D. Brody, "Simulation of Thermal Stresses in Continuous Casting Using a Finite Element Method", Nuclear Metallurgy Vol. 20 (2) 1976, pp. 1138-1150.

30. M. Heinlein, S. Mukherjee, and O. Richmond, "A Boundary Element Method Analysis of Temperature Fields and Stress During Solidification", Acta Mechanica 1986 Vol. 59, Ed. S-Verlag 1986, pp. 59-81.

31. H. Fjaer and A. Mo, "Mathematical Modelling of Thermal Stresses During D.C. Casting of Aluminum Billets", Light Metals 1990, Ed. C. M. Bickert, TMS 1990, pp. 945-950.

32. A. Mo and E.J. Holm, "On the Use of Constitutive Internal Variable Equations for Thermal Stress Predictions in Aluminum Casting", Journal of Thermal Stresses 14 1991, pp. 571-587.

33. M. A. Wells," Mathematical Modelling of the Microstructure and Texture Changes During Hot Tandem Rolling of AA5182 and AA5052 Aluminum Alloys", Ph.D Thesis, UBC 1995, Vancouver Canada, pp. 50.

34. K. P. Rao and E. B Hawbolt," Development of Constitutive Relationships Using Compression Testing of a Medium Carbon Steel" Journal of Engineering Materials and Technology Vol. 114 1992, pp. 116-123.

35. G. E. Dieter, "Mechanical Metallurgy", MacGraw-Hill 2nd Edition, pp. 44-45.

36. ABAQUS Standard User's Manual Vol. 1 Version 5.8. Hibbit Karlsson and Sorenson. Inc 1998.

37. L. F. Mondolfo, " Aluminum Alloys: Structure and Properties, London P Butterworths 1976.

38. Thermomechanical Analysis of the DC Casting Start-Up for Aluminum Sheet Ingot. Internal Report 2000.

39. J. J. Jonas, C. M Sellars and W. J. McG. Tegart, " Hot Workability", International Metallurgical Review 17 (158) 1972, pp. 1-24.

40. C. Zener, J. H. Hollomon, "Effect of Strain Rate Upon Plastic Flow of Steel", Journal of Applied Physics Vol. 15 1944, pp. 22-32.

41. Metals Handbook Ed. J. R. Davis ASM International 1998 Edition.

42. S. Martinez de la Puente, B. Verlinden, L. Delaey, "Hot Workability of an Al-Mg alloy AA5182 with 1 wt % Cu" Journal of Material Science, Ed. Chapman and Hall, 1998, pp. 6167-6173.

APPENDIX A

A1 Method used to convert load displacement data to stress-strain data

If the results of compression and/or tensile testing are to be used to predict how the material will behave under other forms of loading, it is desirable to plot the data in terms of true stress and true strain. To this end the force - displacement data recorded from the test was manipulated mathematically to convert these to stress-strain data for our subsequent analysis.

A1.1 - Determination of true strain
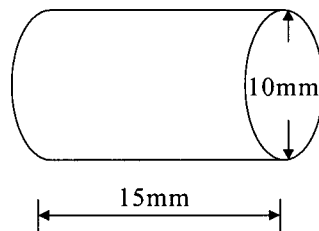
Figure A1.1 - Compression test sample at room temperature
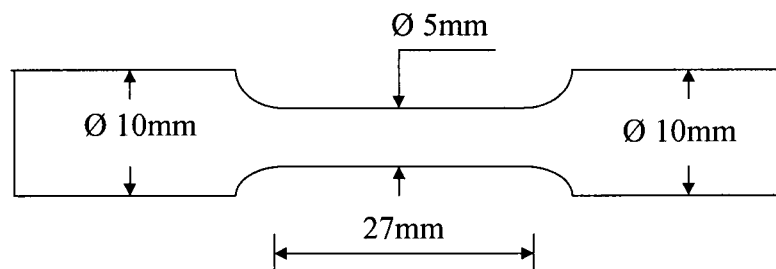
Figure A1.2 - Tensile test sample.
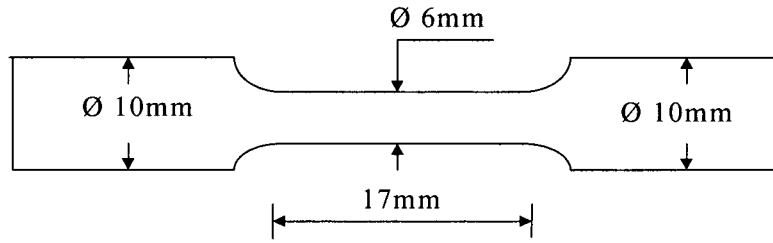
Figure A1.3 - Combination test (cyclic) sample.

The dimensions of the samples at the start of deformation were determined taking into account the variations due to thermal expansion when heated from room temperature up to the deformation temperature. Figures A1.1, A1.2 and A1.3 show the original dimensions of the samples. These dimensional changes were determined from the following relations:

$$D_o = D_{RT} + \delta D_{thermal} \qquad (A1.1)$$

$$L_o = L_{RT} + \delta L_{thermal} \qquad (A1.2)$$

where:

D_o and L_o are the diameter and length respectively at the start of deformation (T_{def})

D_{RT} and L_{RT} are the dimensions at room temperature

$\delta D_{thermal}$ is the change in diameter due to thermal expansion at the deformation temperature

$\delta L_{thermal}$ is the change in length due to thermal expansion at the deformation temperature

Now we determine the volume of the samples, assuming the deformation is uniform and that there is no barreling after deformation. However, barreling was observed after deformation in some of the samples and this when taking into

71

consideration could introduce errors in the calculation of the crosswise strain (from δD) when used to compute the stress and strain.

$$V_o = V \qquad \text{(A1.3)}$$

where:

V_o and V are the volume prior to and after deformation respectively.

Therefore;

$$A_o L_o = A L \qquad \text{(A1.4)}$$

where, the cross-sectional area is determined from the following formulas:

$$A = \pi \cdot r^2 = \pi \cdot \frac{D^2}{4} \qquad \text{(A1.5)}$$

and

$$A = \pi \cdot \frac{D_o^2}{4} = \frac{A_o \cdot L_o}{L} = \frac{V_o}{L} \qquad \text{(A1.6)}$$

where:
L_o is the length at T_{def}, A is the instantaneous cross-sectional area.

Therefore from our assumption of constant volume and uniform deformation and rearranging equations (A1.4) we get:

$$\frac{L}{L_o} = \frac{A_o}{A} \qquad \text{(A1.7)}$$

$$\frac{A_o}{A} = \left(\frac{D_o}{D} \right)^2 \qquad \text{(A1.8)}$$

Now from equation (A1.8) above we can determine the strains as follows:

$$\varepsilon_c = 2\ln\left(\frac{D}{D_0} \right) = 2\ln\left(\frac{10 + \delta D}{D_0} \right) \qquad \text{(A1.9)}$$

$$\varepsilon_L = \ln\left(\frac{L_0}{L} \right) = \ln\left(\frac{L_0}{1.5 - \delta L} \right) \qquad \text{(A1.10)}$$

72

where ε_c and ε_L are the true crosswise and lengthwise strains respectively. The latter gives negative values (compression) but we consider the absolute values.

A1.2 Determination of true stress

The engineering stress-strain curve does not represent a true indication of the deformation characteristics of a material because it is based entirely on the original dimensions of the specimen, and these dimensions changed continuously during the test

$$\sigma = \frac{F}{A} \qquad (A1.11)$$

$$\sigma_A = 9.81 \cdot \frac{Aux.LoadCell}{A} \qquad (A1.12)$$

$$\sigma_F = 9.81 \cdot \frac{S\tan dard.Load.Cell}{A} \qquad (A1.13)$$

where :

A is the instantaneous cross-sectional area and $9.81 \mathrm{ms}^{-2}$ is the acceleration of gravity in order to convert the applied force into unit load with units of stress in MPa.

The graphs shown in Appendix B were finally plotted as true stress and strain using data determined from equations A1.10 and A1.12.

APPENDIX B

B1.1– Strain time curves determined from the compression tests.
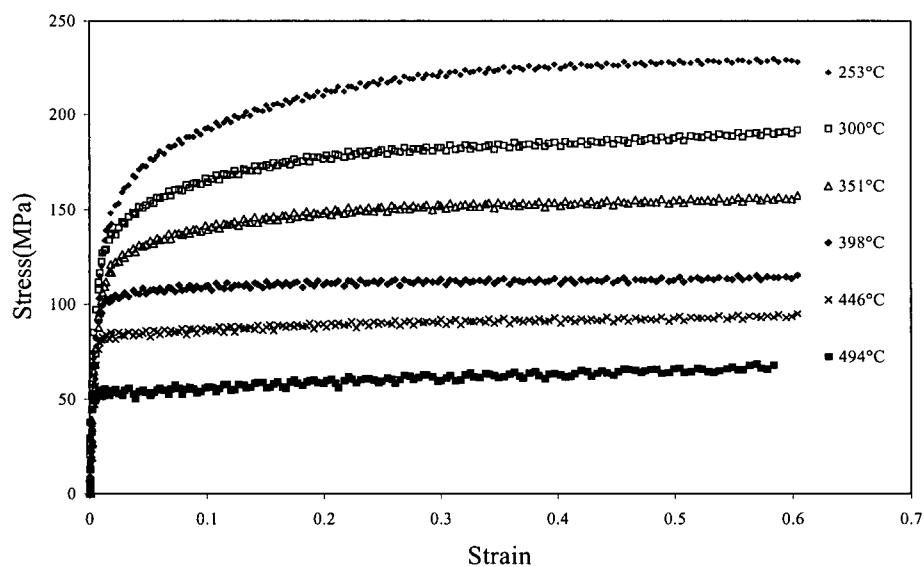
Figure B1.1. Stress-strain curve at a nominal strain rate of 1.0 s^{-1}.
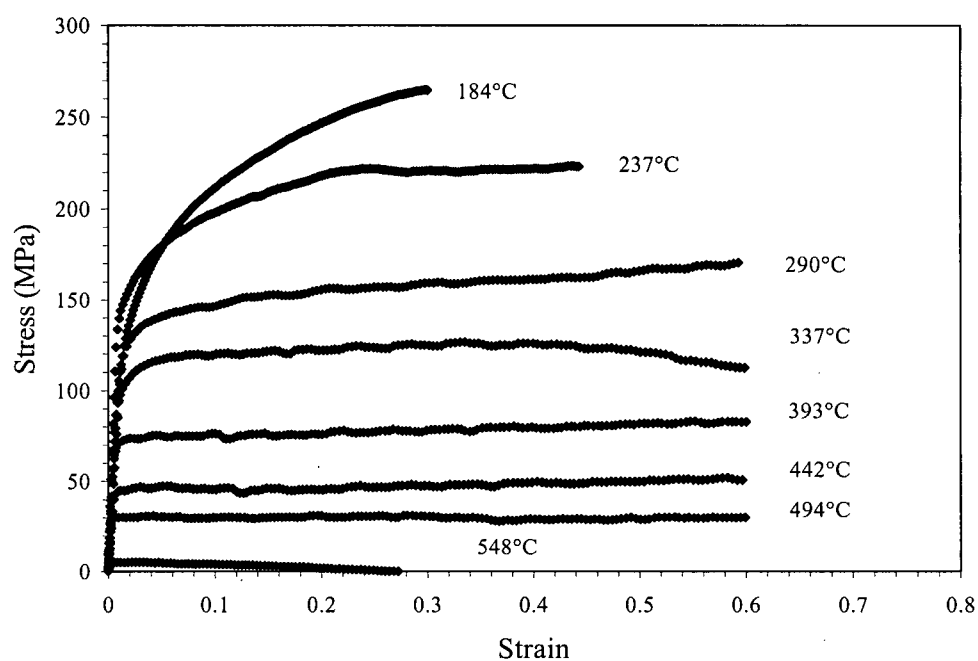
Figure B1.2. Stress-strain curves at a nominal strain rate of 1.0E-1 s^{-1}.
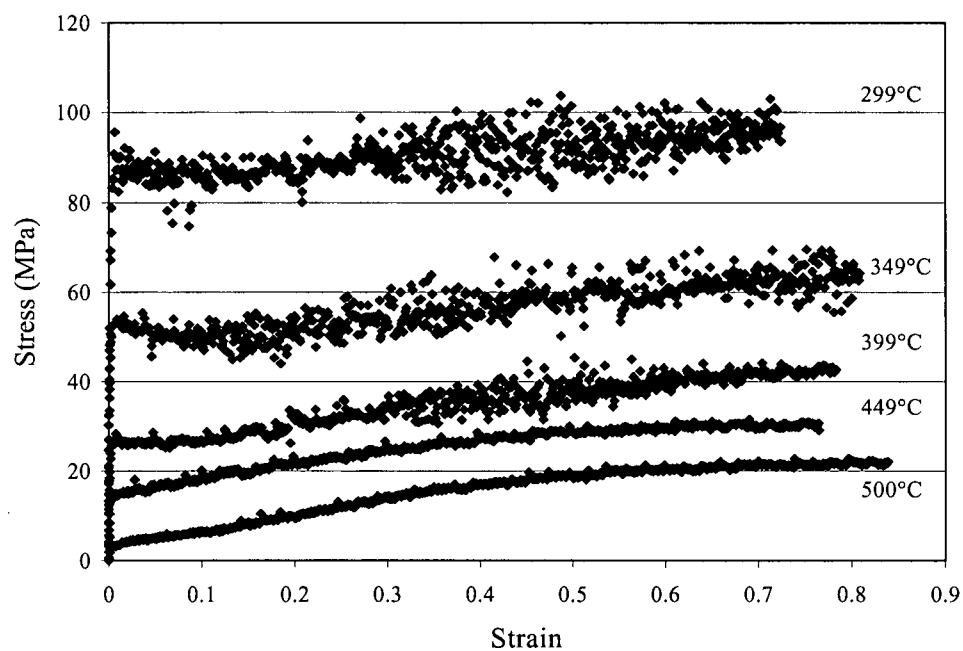
Figure B1.3. Stress-strain curves at a nominal strain rate of 1.0E-3 s^{-1}.

APPENDIX C

C1.1 Compression and Tension Test Results

Table C.1 - Summary of compression test results.

Sample No.	Temperature T_{def} (°C)	Strain Rate (s^{-1})	Measured flow stress (MPa)
1	500	8.6E-06	24.6
2	400	1.1E-05	28.1
3	298	1.1E-05	35.23
4	299	7.6E-4	93.52
5	449	7.6E-4	24.0
6	349	7.8E-4	55.91
7	399	7.9E-4	36.34
8	500	7.4E-4	17.60
9	238	7.2E-2	220.74
10	290	7.6E-2	158.45
11	393	7.7E-2	78.03
12	494	7.9E-2	30.73
13	337	8.0E-2	124.83
14	442	8.1E-2	48.07
15	300	7.2E-1	181.3
16	253	7.4E-1	225.3
17	351	7.6E-1	150.9
18	399	7.6E-1	111.60
19	446	7.7E-1	89.6
20	494	1.02	59.35

Table C.2 Summary of tension test results.

Sample No.	Temperature T_{def} (ºC)	Strain Rate (s^{-1})	Measured flow stress (MPa)
1	297.30	0.0012	131.80
2	397.80	0.0012	65.59
3	299.38	0.109	163.08
4	401.33	0.108	124.76
5	502.37	0.107	74.03
6	247.27	1.036	213.81
7	298.59	0.993	168.74
8	349.66	0.928	145.97
9	400.5	0.931	131.77
10	452.61	0.935	111.15
11	497.68	0.936	86.88

APPENDIX D

Table - D1.1 Mechanical Property Data for AA5182

a) Static flow stress

Temperature (°C)	Strain rate (s^{-1})	Static flow stress (MPa)
245	0.096	130.0
303	0.14	80.0
364	0.10	19.6
402	0.16	12.3
452	0.15	12.6
503	0.12	5.2

b) Plasticity data
Strain rate = 1.0E-5 s^{-1}

Temperature (°C)	Strain rate (s^{-1})	Stress (MPa)	Strain
500	8.6E-6	21	0
500	8.6E-6	22	0.02
500	8.6E-6	23.5	0.04
500	8.6E-6	24.5	0.06
500	8.6E-6	24.5	0.08
500	8.6E-6	25	0.1
500	8.6E-6	25.5	0.2
500	8.6E-6	25.6	0.3
500	8.6E-6	25.6	0.6
500	8.6E-6	25.6	0.8
500	8.6E-6	25.6	1.0

Temperature (°C)	Strain rate (s^{-1})	Stress (MPa)	Strain
400	1.1E-5	24	0
400	1.1E-5	26	0.01
400	1.1E-5	27	0.02
400	1.1E-5	27	0.03
400	1.1E-5	27	0.04
400	1.1E-5	27	0.05
400	1.1E-5	27.5	0.1
400	1.1E-5	27.5	0.15
400	1.1E-5	27	0.25

Temperature (°C)	Strain rate (s^{-1})	Stress (MPa)	Strain
298	1.1E-5	38	0
298	1.1E-5	39	0.01
298	1.1E-5	40	0.02
298	1.1E-5	40	0.03
298	1.1E-5	40	0.04
298	1.1E-5	41	0.05
298	1.1E-5	41.6	0.1
298	1.1E-5	43	0.15
298	1.1E-5	43	0.2
298	1.1E-5	43	0.25
298	1.1E-5	43	0.3

Strain rate = 1.0E-3 s^{-1}

Temperature (°C)	Strain rate (s^{-1})	Stress (MPa)	Strain
500	7.4E-4	16	0
500	7.4E-4	17.5	0.01
500	7.4E-4	18	0.02
500	7.4E-4	18	0.04
500	7.4E-4	18	0.06
500	7.4E-4	18	0.08
500	7.4E-4	18	0.1
500	7.4E-4	18	0.2
500	7.4E-4	18	0.3
500	7.4E-4	18	0.4
500	7.4E-4	18	0.6

Temperature (°C)	Strain rate (s^{-1})	Stress (MPa)	Strain
449	7.6E-4	23	0
449	7.6E-4	23.5	0.01
449	7.6E-4	24	0.02
449	7.6E-4	24	0.04
449	7.6E-4	24	0.06
449	7.6E-4	24	0.08
449	7.6E-4	24	0.1
449	7.6E-4	24	0.2
449	7.6E-4	24	0.3
449	7.6E-4	24	0.4
449	7.6E-4	24	0.6

Temperature (°C)	Strain rate (s⁻¹)	Stress (MPa)	Strain
399	7.9E-4	36	0
399	7.9E-4	37	0.1
399	7.9E-4	37	0.2
399	7.9E-4	37	0.4
399	7.9E-4	37	0.6
399	7.9E-4	37	0.8

Temperature (°C)	Strain rate (s⁻¹)	Stress (MPa)	Strain
349	7.8E-4	52	0
349	7.8E-4	54	0.02
349	7.8E-4	54	0.04
349	7.8E-4	54	0.06
349	7.8E-4	56	0.1
349	7.8E-4	56	0.2
349	7.8E-4	58	0.4
349	7.8E-4	58	0.6

Temperature (°C)	Strain rate (s⁻¹)	Stress (MPa)	Strain
299	7.6E-4	84	0
299	7.6E-4	85	0.02
299	7.6E-4	85	0.04
299	7.6E-4	85	0.06
299	7.6E-4	88	0.1
299	7.6E-4	89	0.2
299	7.6E-4	90	0.4
299	7.6E-4	92	0.6
299	7.6E-4	92	0.8
299	7.6E-4	92	1.0

Strain rate = 1.0E-1 s⁻¹

Temperature (°C)	Strain rate (s⁻¹)	Stress (MPa)	Strain
494	7.9E-2	30	0
494	7.9E-2	31.8	0.01
494	7.9E-2	31.8	0.02
494	7.9E-2	31.8	0.04
494	7.9E-2	31.8	0.06
494	7.9E-2	31.8	0.08
494	7.9E-2	31.8	0.2
494	7.9E-2	31.8	0.4
494	7.9E-2	31.8	0.6

Temperature (°C)	Strain rate (s⁻¹)	Stress (MPa)	Strain
442	8.1E-2	45	0
442	8.1E-2	46	0.01
442	8.1E-2	46	0.02
442	8.1E-2	46	0.04
442	8.1E-2	46	0.06
442	8.1E-2	46	0.08
442	8.1E-2	46	0.2
442	8.1E-2	46	0.4
442	8.1E-2	46	0.5
442	8.1E-2	46	0.6

Temperature (°C)	Strain rate (s⁻¹)	Stress (MPa)	Strain
393	7.7E-2	70	0
393	7.7E-2	72	0.01
393	7.7E-2	74	0.02
393	7.7E-2	74	0.04
393	7.7E-2	76	0.06
393	7.7E-2	76	0.08
393	7.7E-2	76	0.2
393	7.7E-2	80	0.3
393	7.7E-2	80	0.4
393	7.7E-2	82	0.5
393	7.7E-2	82	0.6

Temperature (°C)	Strain rate (s^{-1})	Stress (MPa)	Strain
337	8.0E-2	100	0
337	8.0E-2	104	0.01
337	8.0E-2	108	0.02
337	8.0E-2	116	0.04
337	8.0E-2	118	0.06
337	8.0E-2	120	0.08
337	8.0E-2	120	0.1
337	8.0E-2	124	0.2
337	8.0E-2	124	0.3
337	8.0E-2	124	0.4
337	8.0E-2	124	0.5
337	8.0E-2	124	0.6

Temperature (°C)	Strain rate (s^{-1})	Stress (MPa)	Strain
290	7.6E-2	125	0
290	7.6E-2	132	0.01
290	7.6E-2	136	0.02
290	7.6E-2	138	0.04
290	7.6E-2	140	0.06
290	7.6E-2	144	0.08
290	7.6E-2	148	0.1
290	7.6E-2	152	0.2
290	7.6E-2	158	0.3
290	7.6E-2	160	0.4
290	7.6E-2	164	0.5
290	7.6E-2	164	0.6

Temperature (°C)	Strain rate (s^{-1})	Stress (MPa)	Strain
238	7.2E-2	140	0
238	7.2E-2	150	0.01
238	7.2E-2	160	0.02
238	7.2E-2	170	0.04
238	7.2E-2	195	0.06
238	7.2E-2	200	0.08
238	7.2E-2	200	0.1
238	7.2E-2	205	0.12
238	7.2E-2	205	0.14
238	7.2E-2	210	0.16
238	7.2E-2	215	0.18
238	7.2E-2	220	0.2
238	7.2E-2	220	0.4
238	7.2E-2	220	0.5
238	7.2E-2	220	0.6

Temperature (°C)	Strain rate (s^{-1})	Stress (MPa)	Strain
184	6.7E-2	124	0
184	6.7E-2	138	0.01
184	6.7E-2	157	0.02
184	6.7E-2	182	0.04
184	6.7E-2	197	0.06
184	6.7E-2	209	0.08
184	6.7E-2	218	0.1
184	6.7E-2	226	0.12
184	6.7E-2	234	0.14
184	6.7E-2	241	0.16
184	6.7E-2	246	0.18
184	6.7E-2	251	0.2
184	6.7E-2	261	0.25

Strain rate = 1.0 s⁻¹

Temperature (°C)	Strain rate (s⁻¹)	Stress (MPa)	Strain
494	8.0E-1	50	0
494	8.0E-1	55	0.01
494	8.0E-1	55	0.02
494	8.0E-1	55	0.04
494	8.0E-1	55	0.06
494	8.0E-1	55	0.1
494	8.0E-1	60	0.2
494	8.0E-1	60	0.3
494	8.0E-1	65	0.4
494	8.0E-1	65	0.5
494	8.0E-1	65	0.6

Temperature (°C)	Strain rate (s⁻¹)	Stress (MPa)	Strain
446	7.7E-1	80	0
446	7.7E-1	82	0.01
446	7.7E-1	84	0.02
446	7.7E-1	86	0.04
446	7.7E-1	87	0.06
446	7.7E-1	88	0.1
446	7.7E-1	90	0.2
446	7.7E-1	90	0.3
446	7.7E-1	92	0.4
446	7.7E-1	92	0.5
446	7.7E-1	94	0.6

Temperature (°C)	Strain rate (s⁻¹)	Stress (MPa)	Strain
399	7.6E-1	100	0
399	7.6E-1	104	0.01
399	7.6E-1	106	0.02
399	7.6E-1	108	0.04
399	7.6E-1	110	0.06
399	7.6E-1	110	0.08
399	7.6E-1	110	0.1
399	7.6E-1	112	0.2
399	7.6E-1	112	0.3
399	7.6E-1	112	0.4
399	7.6E-1	112	0.5
399	7.6E-1	112	0.6

Temperature (°C)	Strain rate (s^{-1})	Stress (MPa)	Strain
351	7.6E-1	110	0
351	7.6E-1	110	0.01
351	7.6E-1	120	0.02
351	7.6E-1	124	0.04
351	7.6E-1	132	0.06
351	7.6E-1	136	0.08
351	7.6E-1	140	0.1
351	7.6E-1	142	0.12
351	7.6E-1	145	0.14
351	7.6E-1	147	0.16
351	7.6E-1	148	0.18
351	7.6E-1	148	0.2
351	7.6E-1	150	0.3
351	7.6E-1	155	0.36
351	7.6E-1	155	0.4
351	7.6E-1	155	0.5
351	7.6E-1	155	0.6
351	7.6E-1	155	0.8

Temperature (°C)	Strain rate (s^{-1})	Stress (MPa)	Strain
300	7.2E-1	130	0
300	7.2E-1	140	0.01
300	7.2E-1	150	0.02
300	7.2E-1	155	0.04
300	7.2E-1	160	0.06
300	7.2E-1	160	0.08
300	7.2E-1	165	0.1
300	7.2E-1	180	0.2
300	7.2E-1	182	0.3
300	7.2E-1	185	0.4
300	7.2E-1	188	0.5
300	7.2E-1	190	0.6

Temperature (°C)	Strain rate (s⁻¹)	Stress (MPa)	Strain
253	7.4E-1	150	0
253	7.4E-1	155	0.01
253	7.4E-1	160	0.02
253	7.4E-1	170	0.04
253	7.4E-1	180	0.06
253	7.4E-1	185	0.08
253	7.4E-1	190	0.1
253	7.4E-1	192	0.12
253	7.4E-1	195	0.14
253	7.4E-1	200	0.16
253	7.4E-1	205	0.18
253	7.4E-1	208	0.2
253	7.4E-1	210	0.22
253	7.4E-1	215	0.24
253	7.4E-1	218	0.26
253	7.4E-1	220	0.28
253	7.4E-1	225	0.3
253	7.4E-1	225	0.4
253	7.4E-1	227	0.5
253	7.4E-1	227	0.6

c) Creep data

Hyperbolic sine equation

$$\dot{\varepsilon} = 2.91x10^{11}\left[\sinh\left(0.005\sigma_s\right)\right]^{6.74}\exp\left(-\frac{126,000}{RT}\right)$$

Table - D1.2 - Elastic Property data used in ABAQUS input decks

Young's Modulus E (GPa)	Poisson's Ratio ν	Temperature (°C)
70.973	0.3	20
70.659	0.3	30
70.346	0.3	40
70.032	0.3	50
68.465	0.3	100
65.330	0.3	200
62.195	0.3	300
59.060	0.3	400
47.195	0.3	500

APPENDIX E

E1.1 Determination of Exponents used in Standard Creep-Based Constitutive Laws

E1.1.2 Power law

The Power-law equation (Equation E.1) was used to fit the data in the low stress regime (i.e. $\sigma_s < 48$ MPa).

$$\dot{\varepsilon} = A_1 \sigma_s \exp\left(-\frac{126,000}{RT}\right) \qquad (E.1)$$

Zener and Hollomon [40] suggested that the flow stress at constant strain was related to both the strain rate and the temperature.

$$Z = A_1 \sigma_s^n \qquad (E.2)$$

The quantity Z is the Zener-Hollomon parameter and is also referred to as a *temperature-compensated strain rate*.

$$Z = \dot{\varepsilon} \exp\left(\frac{Q}{RT}\right) \qquad (E.3)$$

where A_1 and n are experimentally determined material alloy-dependent constants and Q is the activation energy for deformation. R and T are the universal gas constant (8.3144J/moleK) and temperature (K) respectively. An activation energy of 126kJ/mole for aluminum was used for the data analysis [41].

$$Z = A_1 \sigma_s^n \qquad (E.4)$$

Rearranging Equation E.4 we are able to determine $\ln \sigma_s$ as follows:

$$\ln \sigma_s = \frac{\ln Z - \ln A_1}{n} \qquad\qquad (E.5)$$

As shown in Figure E1.1, the power law creep equation is able to predict the steady flow stress at low stress values (i.e. $\sigma_{ss} < 48$ MPa) but at high stress values, it under predicts the steady state flow stress.

The parameters were determined from the entire test range spanning both low and high stress regimes. However, for the purposes of illustrating the difference between the various constitutive laws, we selected a threshold stress of 48 MPa below which we curve fit the power-law and above which the exponential relation was fit.
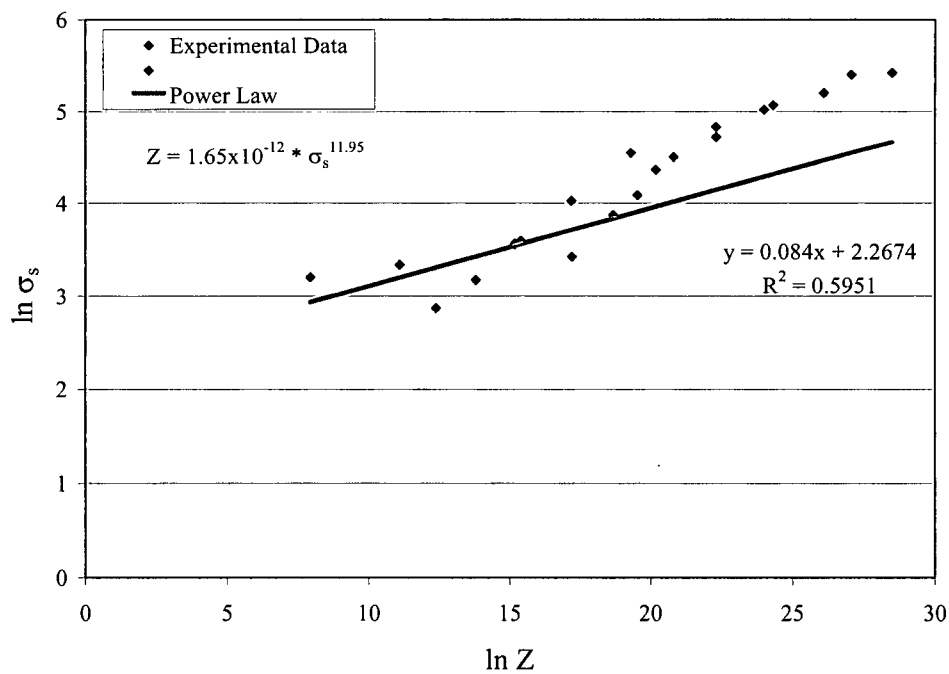

Figure E1.1. - Experimental data fit by Power-law equation.

E1.1.3 Exponential equation

The Exponential equation, is a creep based equation which is able to more accurately predict the steady state flow stress at higher stress levels (i.e., > 48 MPa). This equation was used to analyze the data for higher steady state flow stresses measured for AA5182. The exponential equation is shown below in Equation E.6.

$$\dot{\varepsilon} = A_2 \exp(\beta\sigma_s)\exp\left(-\frac{Q}{RT}\right) \qquad (E.6)$$

Replacing the Zener-Hollomon parameter into the equation gives the following:

$$Z = A_2 \exp(\beta\sigma_s) \qquad (E.7)$$

$$\ln Z = \ln A_2 + \beta\sigma_s \qquad (E.8)$$

Rearranging terms in equation E.8:

$$\sigma_s = \frac{\ln Z - \ln A_2}{\beta} \qquad (E.9)$$

As shown in Figure E1.2, the exponential equation is capable of predicting the steady state flow stress and high values of Z but at low values of Z it under predicts the flow stress.

$Z = 4.16 \times 10^6 \exp(0.058 * \sigma_s)$

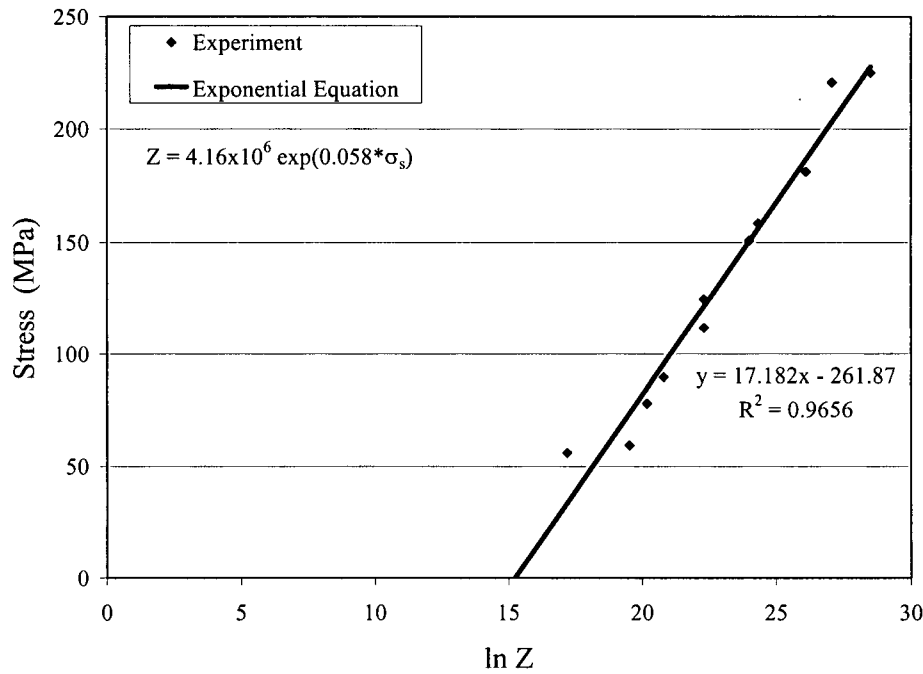$y = 17.182x - 261.87$
$R^2 = 0.9656$

Figure E1.2. - Experimental data fit by exponential equation

E1.1.4 Hyperbolic-sine equation

Several researchers have found the hyperbolic-sine equation proposed by Sellars and Tegart [6,17,30,41] to be particularly useful for correlating flow stress, temperature and strain rate under hot working conditions for aluminum and its alloys. The hyperbolic-sine equation is shown below:

$$\dot{\varepsilon} = A_3 [\sinh(\alpha \sigma_s)]^m \exp\left(-\frac{Q}{RT}\right) \qquad \text{(E.10)}$$

where A_3, α and m are experimentally determined alloy-dependent constants and Q is the activation energy for deformation. At low stresses (i.e., $\alpha\sigma < 1.0$) Equation E.10 reduces to a power relation and at high stresses (i.e., $\alpha\sigma > 1.2$) it reduces to an exponential relation.

91

Replacing the Zener-Hollomon parameter into the equation gives:

$$Z = A_3 \left[\sinh(\alpha \sigma_s) \right]^m \qquad \text{(E.11)}$$

and taking the ln of both sides:

$$\ln Z = \ln \dot{\varepsilon} + Q/RT = \ln A_3 + m \ln \left[\sinh(\alpha \sigma_s) \right] \qquad \text{(E.12)}$$

Now rearranging the terms in Equation E.12, we have

$$\ln Z = \ln \dot{\varepsilon} + Q/RT = \ln A_3 + m \ln \left[\sinh(\alpha \sigma_s) \right] \qquad \text{(E.13)}$$

where:

$$\ln \left[\sinh(\alpha \sigma_s) \right] = \frac{\ln Z}{m} - \frac{\ln A_3}{m} = U \qquad \text{(E.14)}$$

and

$$\sinh(\alpha \sigma_s) = \exp(U) = V \qquad \text{(E.15)}$$

finally we can predict the flow stress as:

$$\sigma_s = \frac{a \sinh(V)}{\alpha} \qquad \text{(E.16)}$$

where the value of $\alpha = \dfrac{\beta}{n} = 0.005$ has been determined from Power-law and Exponential

equations.

As shown in Figure E1.3, the hyperbolic sine equation is able to predict the flow stress for both low and high stress conditions.

$Z = 2.92\text{x}10^{11}[\text{Sinh}(0.005 * \sigma_s)]^{6.74}$

$y = 0.1482x - 3.9129$
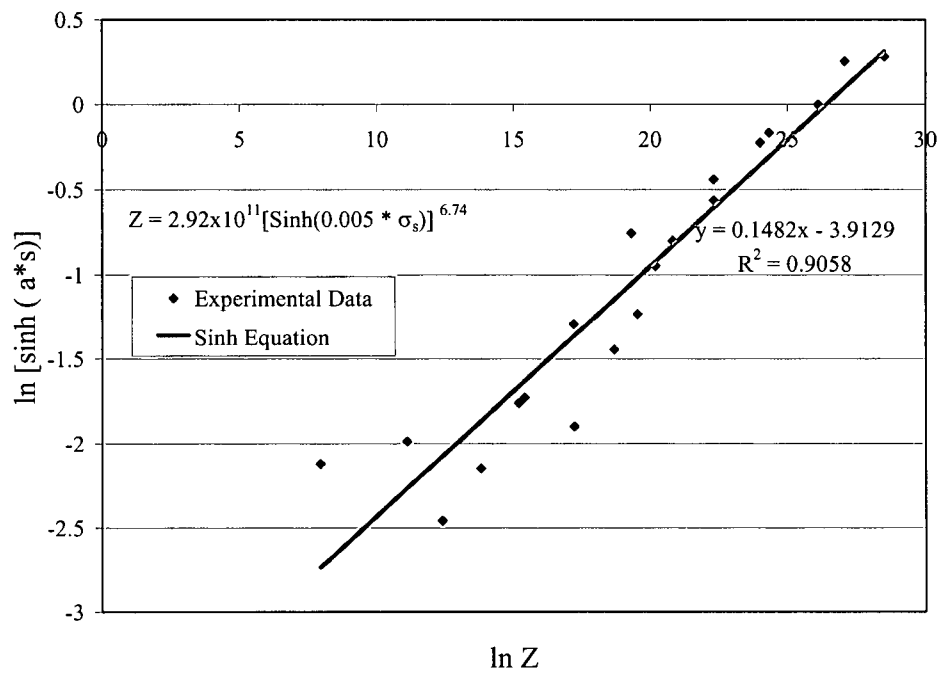$R^2 = 0.9058$

- ◆ Experimental Data
- —— Sinh Equation

Figure E1.3. Experimental data fit by hyperbolic-sine equation

93